

1   **Mitotic gene bookmarking by RUNX1 contributes to stabilization of the normal  
2   mammary epithelial phenotype**

3   Joshua T. Rose<sup>1</sup>, Joseph R. Boyd<sup>1</sup>, Jonathan A. Gordon<sup>1</sup>, Mingu Kang<sup>1</sup>, Eliana  
4   Moskovitz<sup>1</sup>, Nicole A. Bouffard<sup>2</sup>, Andrew J. Fritz<sup>1</sup>, Anuradha Illendula<sup>3</sup>, John H.  
5   Bushweller<sup>3</sup>, Jane B. Lian<sup>1</sup>, Janet L. Stein<sup>1</sup>, Gary S. Stein<sup>1</sup>, and Sayyed K. Zaidi<sup>1\*</sup>

6

7   <sup>1</sup>Department of Biochemistry and University of Vermont Cancer Center, Robert Larner  
8   College of Medicine, 89 Beaumont Avenue, Burlington, VT 05405, USA

9   <sup>2</sup>Microscopy Imaging Center at the Robert Larner College of Medicine, 89 Beaumont  
10   Avenue, Burlington, VT 05405, USA

11   <sup>3</sup>Department of Molecular Physiology and Biological Physics, University of Virginia,  
12   Charlottesville, VA 22908, USA

13

14   \*Corresponding Author

15   Sayyed K Zaidi, PhD

16   [sayyed.zaidi@med.uvm.edu](mailto:sayyed.zaidi@med.uvm.edu)

17   Room E210, Given Building

18   University of Vermont

19   89 Beaumont Avenue, Burlington VT 05405

20

21   **Key Words:** Mammary phenotype, epithelial phenotype, RUNX1, mitotic gene  
22   bookmarking.

23   **Summary Statement**

24       This study elucidates mitotic gene bookmarking as a novel epigenetic mechanism  
25   in breast epithelial cells which impacts cell growth and phenotype and has potential  
26   implications in breast cancer onset.

27 **Abstract**

28 Loss of the RUNX1 transcription factor leads to epithelial-to-mesenchymal  
29 transition (EMT), but mechanisms by which RUNX1 stabilizes the mammary epithelial  
30 phenotype are not known. Here, we report RUNX1 gene bookmarking during mitosis as  
31 one of the key epigenetic mechanisms to convey regulatory information for coordinate  
32 control of mammary cell proliferation, growth, and identity through successive cell  
33 divisions. Genome-wide RUNX1 occupancy profiles for asynchronous, mitotically-  
34 enriched, and G1 breast epithelial cells reveal RUNX1 is retained during mitosis on RNA  
35 Pol I- (i.e., ribosomal RNA) and II-transcribed protein coding (e.g., *HES1*) and long non-  
36 coding RNA (e.g., *NEAT1*) genes controlling proliferation, growth, and mammary  
37 epithelial phenotype maintenance. Disruption of RUNX1 DNA binding and target gene  
38 occupancy alters cell morphology, global protein synthesis, and phenotype-related gene  
39 expression. Together, these findings demonstrate that RUNX1 mitotic bookmarking  
40 contributes to maintenance of the normal mammary epithelial phenotype. Compromising  
41 RUNX1 DNA binding initiates EMT, an essential first step in the onset of breast cancer.

42           Breast cancer arises from a series of acquired mutations and epigenetic changes  
43        that disrupt normal mammary epithelial homeostasis and create multi-potent cells that  
44        can differentiate into biologically unique clinically distinct subtypes. Epithelial-to-  
45        mesenchymal transition (EMT) – a trans-differentiation process through which mammary  
46        epithelial cells acquire an aggressive mesenchymal phenotype – is a key driver of breast  
47        cancer progression, invasion and metastasis <sup>1</sup>. Transcription factors Snail, Slug, Twist,  
48        and Zeb1/2 contribute to EMT during early, normal development and have also been  
49        implicated in invasion <sup>2-5</sup>. Despite accumulating evidence for a broad understanding of  
50        EMT regulation and maintenance of the epithelial phenotype, the mechanism(s) by which  
51        mammary epithelial cells maintain their biological phenotype is unknown.

52           Runt-Related Transcription Factor 1 (RUNX1/AML1) is required for hematopoietic  
53        lineage specification during development and hematopoiesis throughout life <sup>6-19</sup>. In  
54        addition to the recognized role in hematological malignancies, RUNX1 has been recently  
55        identified as a key player in breast cancer development and tumor progression <sup>20-24</sup>.  
56        RUNX1 is significantly mutated in breast tumors <sup>25-27</sup>. Findings from our group, reinforced  
57        by studies from others, have shown that RUNX1 maintains breast epithelial phenotype  
58        and prevents EMT through transcriptional regulation of genes involved in key cellular  
59        pathways <sup>23</sup>. This regulation is reflected by RUNX1 control of E-cadherin expression, a  
60        key cell adhesion protein and marker of EMT <sup>28</sup>. Consequently, there is a requirement to  
61        understand epigenetic mechanisms by which RUNX1 stabilizes the normal mammary  
62        epithelial phenotype.

63           Mitotic gene bookmarking, i.e. transcription factor binding to target genes during  
64        mitosis for transcriptional regulation following cell division, is a key epigenetic mechanism

65 to convey and sustain regulatory information for cell proliferation, growth, and cell identity  
66 from parent to progeny cells<sup>29-31</sup>. Phenotypic transcription factors that include GATA1,  
67 RBPJ, FoxA1, SOX2, OCT4, and KLF4, bookmark target genes during mitosis<sup>32-36</sup>. We  
68 have established that RUNX proteins as well as other phenotypic transcription factors  
69 that include MYOD and CEBPα bookmark RNA Pol I- and II-transcribed genes during  
70 mitosis for coordinate control of cell growth, proliferation and phenotype.<sup>37-40</sup>

71 We addressed the hypothesis that RUNX1 maintains the breast epithelial  
72 phenotype by mitotic bookmarking of genes that support mammary epithelial proliferation,  
73 growth, and phenotype during mitosis for expression immediately after cell division.  
74 Immunofluorescence confocal microscopy revealed that RUNX1 is present on  
75 chromosomes throughout mitosis and colocalizes with upstream binding transcription  
76 factor (UBF), a subunit of RNA Pol I transcriptional machinery. To identify genes occupied  
77 by RUNX1, we performed chromatin immunoprecipitation coupled with high throughput  
78 sequencing (ChIP-Seq) using a RUNX1-specific antibody on mitotic, G1, and  
79 asynchronous normal mammary epithelial MCF10A cells. ChIP-Seq revealed that, in  
80 mitosis, RUNX1 associates with RNA Pol II regulated genes specifically involved in  
81 maintenance of the epithelial phenotype and EMT progression. Interestingly, ribosomal  
82 RNA genes, regulated by the RNA Pol I transcriptional machinery, were occupied by  
83 RUNX1. A fluorescence-based, global protein synthesis assay showed reduced protein  
84 synthesis when RUNX1 DNA binding was perturbed using a small molecule inhibitor.  
85 Strikingly, inhibition of RUNX1 resulted in loss of the epithelial phenotype and acquisition  
86 of mesenchymal properties. These findings establish mitotic gene bookmarking as a key  
87 mechanism for RUNX1 stabilization of the normal breast epithelial phenotype.

88 Importantly, disruption of RUNX1 mitotic bookmarking initiates EMT, an early event in the  
89 onset of breast cancer.

90

91 **RESULTS**

92 **RUNX1 associates with mitotic chromatin and occupies target genes**

93 To investigate subcellular localization of RUNX1 in normal mammary epithelial  
94 cells, we performed immunofluorescence microscopy in actively proliferating MCF10A  
95 cells. We observed that RUNX1 is distributed in punctate subnuclear domains throughout  
96 interphase nuclei (Fig. 1; the Interphase panel). Interestingly, RUNX1 is localized on  
97 mitotic chromatin at all topologically identified substages of mitosis (Fig 1; top panels).  
98 Two distinct types of foci are detectable on mitotic chromosomes: 2-8 large punctate foci  
99 that appear to be allelic as well as numerous smaller foci that were distributed across the  
100 chromosomes (Fig 1; bottom panels, white arrowheads). In agreement with our previous  
101 findings, RUNX1 foci are equally distributed into resulting progeny cells <sup>40</sup>. Presence of  
102 RUNX1 at all stages of mitosis indicates that the protein is stable during cell division.

103 To experimentally address RUNX1 occupancy of target genes, MCF10A cells were  
104 synchronized in mitosis using nocodazole (50ng/mL); additionally, cells in the G1 cell  
105 cycle stage was collected following a 3hr release from the block (Fig. 2A). Mitotic purity  
106 of harvested cells was confirmed by the presence of H3pS28 (>99%; data not shown).  
107 Western blot analysis of whole cell lysates from the three cell populations show expected  
108 levels of expression for cell cycle-specific proteins Cyclin B and CDT1 (Fig. 2B). FACS  
109 profiles of cell populations confirmed the characteristic enrichment of blocked cells in  
110 mitosis (Fig 2C; Mitotic) and release into G1 upon media replacement (Fig 1C; G1) when

111 compared to asynchronous cells (Fig 2C; Asynch). Consistent with immunofluorescence  
112 observations, RUNX1 was present in all three cell populations (Supplement Fig. 1).  
113 Together, these results demonstrate that RUNX1 is stable through mitosis and localizes  
114 to mitotic chromatin.

115 We next determined if RUNX1 remains bound to target genes during mitosis, ChIP-  
116 Seq was performed on Asynch, Mitotic, and G1 MCF10A cells using a RUNX1 specific  
117 antibody (Fig. 2D). Sequencing datasets were mapped to the latest human genome build  
118 (hg38) using Bowtie2. Enriched regions were determined using Model-Based Analysis of  
119 ChIP-Seq (MACS) and were analyzed at  $p < 10^{-5}$  significance level with an irreproducible  
120 discovery rate (IDR) of 0.05. Heatmaps of RUNX1-occupied genes in all three cell  
121 populations were generated by seqsetvis (Bioconductor) (Fig 2D). Comparison of the  
122 three cell populations revealed subsets of genes that were either shared (354 genes)  
123 across the three groups or were specific for each, indicating dynamic binding of RUNX1  
124 during and immediately after mitosis (Fig 2D). Peak calling identified RUNX1 occupancy  
125 of both protein coding and long non-coding RNA (lncRNA) genes. Specifically, RUNX1  
126 occupied 2020 genes in Asynch population (Fig 2D; green bar) and 1095 genes G1-  
127 enriched cells (Fig 2D; light brown bar). Importantly, RUNX1 occupied 551 genes (413  
128 protein coding and 138 lncRNAs) in mitotically-enriched MCF10A cells (Fig 2D; blue bar).

129 Functional relevance of RUNX1 occupancy in the three cell populations was  
130 determined by comparing RUNX1-occupied genes with those that are differentially  
131 regulated upon shRNA-mediated RUNX1 knockdown<sup>23</sup>. Critically important to our central  
132 hypothesis that RUNX1 mitotically bookmarks genes for regulation immediately after cell  
133 division and as shown in Fig 2D, 399 of 1268 RUNX1-bookmarked genes in the M and

134 G1 populations were deregulated upon RUNX1 depletion. These findings reveal that  
135 several hundred target genes are bookmarked by RUNX1 during mitosis and  
136 transcriptionally regulated in normal mammary epithelial cells. To identify cellular  
137 processes and pathways that comprise of RUNX1-bookmarked genes, we performed  
138 gene set enrichment analysis (GSEA) on genes bound by RUNX1 during mitosis or G1,  
139 or not bound in either cell cycle stage (Fig 2E). Interestingly, most genes bookmarked by  
140 RUNX1 during mitosis were associated with negative regulation of gene expression and  
141 metabolic process (Fig 2E; blue box). Consistent with cellular requirement to reattach and  
142 enter the next cell cycle and fully resume transcription, genes bound during G1 were  
143 primarily enriched in biological processes involving cell anchorage, protein localization  
144 and positive regulation of gene expression (Fig 2E; brown box). ChIP-seq results were  
145 further validated by motif analysis of RUNX1-bound peaks, which showed that RUNX  
146 motif was the top enriched motif in all three cell populations (Fig 2F). Importantly, RUNX1-  
147 bound genomic regions were also enriched in motifs for transcription factors known to  
148 cooperate with RUNX1 for gene regulation<sup>41</sup> (Fig 2F). Together, these findings indicate  
149 that RUNX1 bookmarks genes involved in cell proliferation, growth, and phenotype in  
150 normal mammary epithelial cells.

151

## 152 **RUNX1 mitotically bookmarks RNA Pol I-transcribed genes that control cell growth**

153 Our ChIP-Seq results revealed that RUNX1 occupies rDNA repeats in MCF10A  
154 mammary epithelial cells; all three MCF10A cell populations (Asynch, Mitotic and G1)  
155 exhibited significant fold enrichment within the promoter region of hrDNA (Fig 4A),  
156 suggesting a potential role for RUNX1 in regulating rRNA genes in MCF10A cells. We

157 confirmed this finding in actively proliferating MCF10A cells by immunofluorescence  
158 microscopy for antibodies specific against RUNX1 and upstream binding factor (UBF), a  
159 transcriptional activator that remains bound to rRNA genes during mitosis. We observed  
160 large RUNX1 foci colocalizing with UBF throughout each stage of mitosis (Fig 3A; bottom  
161 panels). Colocalization between RUNX1 and UBF was validated by confocal microscopy.  
162 Line scans of MCF10A cells show that although RUNX1 and UBF occupy distinct nuclear  
163 microenvironments in interphase (n=15), both proteins substantially colocalize in  
164 metaphase (n=15) (Fig 3B). Taken together, these findings establish RUNX1 binding to  
165 ribosomal DNA repeat regions identified by ChIP-Seq (Fig 4A) and confirmed at the  
166 cellular level by confocal microscopy (Fig 3).

167 We experimentally addressed the hypothesis that RUNX1 regulates ribosomal  
168 gene expression by using a pharmacological inhibitor of RUNX1. The small molecule  
169 inhibitor—AI-14-91—interferes with RUNX1-CBF $\beta$  interaction and disrupts RUNX1 DNA  
170 binding<sup>42,43</sup>. We first determined the effect of RUNX1 inhibitor on mitotic retention of the  
171 protein. Actively proliferating MCF10A cells were treated with the inhibitor (AI-14-91) for  
172 6hr, 12hr, 24hr, and 48hr at 20 $\mu$ M; a structurally equivalent inert compound (AI-4-88) was  
173 used as a control under identical conditions. Cells were subjected to immunofluorescence  
174 microscopy followed by detection of RUNX1 and UBF as described above. Although  
175 RUNX1 signal was detected in all mitotic sub-stages (data not shown), we observed a  
176 substantial decrease in RUNX1 signal intensity on mitotic chromosomes (white arrows;  
177 Fig 4B), indicating that RUNX1-Cbf $\beta$  interaction and RUNX1 DNA binding activity plays a  
178 key role in mitotic gene bookmarking. These changes were more pronounced for smaller  
179 RUNX1 foci and were not observed in control-treated cells; appreciable signal for large

180 RUNX1 foci that colocalize with UBF (Fig 3) remained detectable in all sub-stages of  
181 mitosis (Fig 4B and data not shown).

182 We next examined the effect of RUNX1 inhibitor on pre-rRNA expression and  
183 found that pre-rRNA expression was significantly increased at 12hr and 48hr timepoints  
184 after treatment of asynchronous cells with specific RUNX1 inhibitor but not inactive  
185 compound, indicating that RUNX1 suppresses rRNA gene expression in normal  
186 mammary epithelial cells (Fig 4C). Because levels of rRNA directly correlate with global  
187 protein synthesis, a fluorescent-based detection method was used to measure newly  
188 synthesized proteins. Cells treated with AI-14-91 for 24hr or 48hr showed a moderate  
189 change in levels of global protein synthesis in comparison to control-treated cells under  
190 identical conditions (Fig 4D). Together, our results demonstrate that RUNX1 bookmarks  
191 RNA Pol I regulated rRNA genes during mitosis and transcriptionally represses them with  
192 moderate impact on global protein synthesis in normal mammary epithelial cells.

193

194 **RUNX1 mitotically bookmarks RNA Pol II-transcribed genes involved in hormone-  
195 responsiveness and cell phenotype**

196 Using RUNX1-bookmarked genes, gene set enrichment analysis (GSEA) was  
197 performed to identify regulatory pathways (Fig 5A). In agreement with known roles of  
198 RUNX1<sup>44-48</sup>, top 10 pathways identified were those involved in regulation of G2M  
199 Checkpoint, E2F targets, p53, and DNA repair (Fig 5A). Consistent with our finding that  
200 RUNX1 bookmarked and regulates rRNA genes, one of the pathways identified is mTOR  
201 signaling, a pathway that is required for cell growth and is a therapeutic target in breast  
202 cancers<sup>49,50</sup>. Relevant to the normal mammary epithelial phenotype, both early and late

203 estrogen response signaling gene sets significantly overlap with RUNX1 mitotically  
204 bookmarked genes (Fig 5A). Because estrogen plays vital roles in promoting proliferative  
205 phenotypes of mammary epithelial cells<sup>51-53</sup>, we interrogated RUNX1 bookmarked genes  
206 to identify those bound by RUNX1 and ERα (Fig 5B)<sup>54</sup>. Using publicly available datasets  
207 of ERα genome-wide occupancy and estradiol-regulated gene expression, we find that a  
208 subset of genes mitotically bookmarked by RUNX1 is also bound by ERα, and either up  
209 or down regulated in response to estradiol. These findings indicate that RUNX1-  
210 bookmarked genes are involved in pathways that control hormone-responsiveness,  
211 proliferation and growth of normal mammary epithelial cells (Fig 5B).

212 A subset of RUNX1-bookmarked genes relates to regulatory pathways involved in  
213 cellular phenotype including TNFα, Apical Junction and Notch signaling (Fig 5A).  
214 Furthermore, NEAT1 and MALAT1, lncRNAs often deregulated in breast cancer<sup>55,56</sup>,  
215 were also mitotically bookmarked by RUNX1. Of the 413 RUNX1 bookmarked protein  
216 coding genes, *TOP2A*, *MYC*, *HES1*, *RRAS*, *H2AFX*, and *CCND3* are representative of  
217 RNA Pol II-transcribed genes involved in phenotype maintenance and cell fate decisions  
218 (See Supplemental Table 1 for complete list). Recently, *HES1* and *H2AFX* have been  
219 identified as regulators of breast epithelial phenotype<sup>57-59</sup>. In our ChIP-seq dataset, *HES1*  
220 and *H2AFX* show significant fold enrichment of RUNX1 occupancy between the three  
221 populations of MCF10A cells (Fig 5C; top panels). Expression of *HES1* increased upon  
222 inhibition of RUNX1 DNA binding (Fig 5C; left panel—bar graph), indicating that RUNX1  
223 represses *HES1*. In contrast, *H2AFX* expression at 24hr and 48hr of inhibitor treatment  
224 was decreased, suggesting RUNX1 activates H2AFX expression (Fig 5C; right panel—  
225 bar graph). These results indicate that by bookmarking both protein coding and non-

226 coding genes that are critical determinants of lineage identity, RUNX1 stabilizes the  
227 mammary epithelial phenotype.

228

229 **Inhibition of RUNX1 DNA binding causes epithelial to mesenchymal transition**

230 To experimentally address whether disruption of RUNX1 bookmarking leads to a  
231 change in epithelial phenotype, we treated cells with RUNX1 DNA binding inhibitor and  
232 monitored changes in cell morphology (Fig 6). Consistent with RUNX1 bookmarking and  
233 regulation of genes critical for epithelial phenotype (Fig 5), disruption of RUNX1 DNA  
234 binding resulted in mesenchymal morphology. We next examined whether long-term  
235 inhibition of RUNX1 caused a permanent change in cell phenotype. Longer term  
236 treatment (5 days) of actively proliferating MCF10A cells showed significant apoptosis,  
237 although a small sub-population of cells survived and exhibited an altered phenotype (Fig  
238 6B). The surviving sub-population at day 5 was recovered by culturing cells in media  
239 without the inhibitor. By day 3-4 following media replacement, cells clearly showed a  
240 mesenchymal morphology (Fig 6B), indicating that interfering with RUNX1 mitotic  
241 bookmarking causes loss of the normal mammary epithelial phenotype. Consistent with  
242 changes in cell morphology, we find alterations in expression and localization of the  
243 cytoskeletal F-actin protein (Fig 6C). These observations were confirmed by examining  
244 the expression of epithelial markers (e.g., E Cadherin (Fig 6D)), as well as mesenchymal  
245 markers (e.g., SNAI2 (Fig 6E)). E-cadherin was partially downregulated, while SNAI2  
246 expression was significantly increased, confirming an epithelial-to-mesenchymal  
247 transition upon inhibition of the RUNX1-Cbf $\beta$  interaction. The p21 gene, a known target  
248 that is repressed by RUNX1, was included as a control and, as expected, showed an

249 increased expression with the inhibitor treatment (Fig 6E; right panel). Together, these  
250 findings show that RUNX1 mitotic bookmarking of epithelial cell growth, proliferation, and  
251 lineage-related genes is a key epigenetic mechanism required to stabilize the normal  
252 mammary epithelial phenotype. Disruption of RUNX1 gene bookmarking results in an  
253 epithelial-to-mesenchymal transition, a key first event at the onset of breast cancer.

254 **DISCUSSION**

255 This study identifies RUNX1 mitotic bookmarking as a novel epigenetic mechanism  
256 for coordinate regulation of RNA Pol I- and II-transcribed genes that are critical for  
257 mammary epithelial proliferation, growth, and phenotype maintenance. Pharmacological  
258 inhibition of RUNX1 DNA binding causes transition to a mesenchymal phenotype,  
259 indicating that RUNX1 bookmarking of target genes contributes to stabilizing the normal  
260 breast epithelial phenotype.

261 Our findings are the first to identify coordinate control of cell growth-related  
262 ribosomal RNA (rRNA) genes and a large subset of cell proliferation/phenotype-related  
263 genes by RUNX1 in normal mammary epithelial cells. In addition to RUNX1 bookmarking  
264 of RNA Pol I-transcribed rRNA genes, RUNX1 is mitotically retained on RNA Pol II-  
265 transcribed genes that are important in breast epithelial cell growth and phenotype. One  
266 target gene of interest is hairy and enhancer of split-1 (*HES1*). Hes1 is a transcription  
267 factor which represses genes involved in cellular development, and is regulated primarily  
268 by NOTCH signaling, one of our top ten overlapping hallmark gene sets bookmarked by  
269 RUNX1 (Fig 5)<sup>60,61</sup>. *HES1* was recently shown to have a prominent role in proliferation  
270 and invasion of breast cancer cells, and its silencing led to a downregulation of p-Akt  
271 signaling and ultimately prevented EMT<sup>57</sup>. Our findings indicate that RUNX1 stabilizes  
272 the normal mammary epithelial phenotype, in part, by bookmarking *HES1* and  
273 suppressing its expression.

274 Another important RNA Pol II-transcribed gene mitotically bookmarked by RUNX1  
275 and critical for maintaining cellular phenotype is histone variant H2AFX (*H2AFX*).  
276 Silencing *H2AFX* in breast epithelial cells leads to induction of EMT through activation of

277 *SNAI2/SLUG* and *TWIST1*<sup>59</sup>. We find a decrease in *H2AFX* expression and a  
278 concomitant, significant increase in *SNAI2/SLUG* expression upon inhibition of the  
279 RUNX1-Cbf $\beta$  interaction. These data identify RUNX1 as a novel upstream regulator of  
280 *H2AFX* expression; RUNX1 bookmarking and activation of *H2AFX* and subsequent  
281 suppression of *SNAI2/SLUG* prevents EMT in breast epithelial cells.

282 Several groups have shown that RUNX1 interacts with ER $\alpha$  at both enhancer  
283 regions and transcriptional start sites (TSSs) for regulation of specific genes<sup>22,54</sup>. Our  
284 ChIP-Seq results, coupled with publicly available data sets, reveal a novel finding: RUNX1  
285 bookmarking of a subset of ER $\alpha$ -occupied, hormone-responsive genes, during mitosis  
286 may be critical for maintenance of breast epithelial phenotype. Future studies will be  
287 required to investigate mechanistic significance of this observation.

288 Our findings are the first to demonstrate that mitotic gene bookmarking contributes  
289 to stabilizing the mammary epithelial phenotype. Equally important, our study shows that  
290 inhibition of RUNX1 DNA binding specifically elicits an epithelial-to-mesenchymal  
291 transition, indicating that mitotic gene bookmarking is a central epigenetic mechanism by  
292 which RUNX1 maintains the epithelial phenotype. These findings are further supported  
293 by RUNX1 mitotic occupancy of cell growth-related rRNA genes, and together highlight  
294 key role(s) of RUNX1 in coordinating cell proliferation, growth and phenotype. Another  
295 novel contribution of the current study is mitotic bookmarking of lncRNAs by a  
296 transcription factor. RUNX1 was recently shown to regulate lncRNAs NEAT1 and NEAT2  
297 (*MALAT1*)<sup>55,62</sup>, lncRNAs with critical roles in the onset and progression of breast cancer<sup>56</sup>.  
298 Our findings show that, in addition to bookmarking protein coding genes, RUNX1  
299 bookmarks several lncRNAs for post-mitotic regulation. It will be important to identify G1-

300 specific roles of RUNX1-bookmarked lncRNAs in maintaining the normal mammary  
301 epithelial phenotype and/or in the onset and progression of breast cancer.

302 In summary, this study establishes a novel epigenetic mechanism where RUNX1  
303 mitotically bookmarks RNA Pol I- and II-transcribed genes for coordinate regulation of  
304 normal mammary epithelial proliferation, growth, and phenotype. Disruption of RUNX1  
305 DNA binding leads to epithelial-to-mesenchymal transition, a key event in breast cancer  
306 onset, and validates the contribution of RUNX1 bookmarking to physiologically sustain  
307 the mammary epithelial phenotype.

308

309

310 **MATERIALS AND METHODS**

311 **Cell Culture Techniques**

312 Breast epithelial (MCF10A) cells were cultured in DMEM/F-12 50/50 mixture  
313 (Corning™, Corning, NY). Culturing media was also supplemented with horse serum to  
314 5% (GIBCO, Grand Island, NY), human insulin to 10 $\mu$ g/mL (Sigma Aldrich, St. Louis, MO),  
315 human epidermal growth factor to 20ng/mL (PeproTech, Rocky Hill, NJ), cholera toxin to  
316 100ng/mL (Thomas Scientific, Swedesboro, NJ), hydrocortisone to 500ng/mL (Sigma  
317 Aldrich, St. Louis, MO), Penicillin-Streptomycin to 100U/mL (Thermo Fisher Scientific,  
318 Ashville, NC), and L-Glutamine to 2mM (Thermo Fisher Scientific, Ashville, NC).

319 For mitotic arrest of parental MCF10A cells, culturing media was supplemented  
320 with 50ng/mL of Nocodazole (Sigma Aldrich, St. Louis, MO) and incubated with cells for  
321 16hrs. Supplementing culturing media with equivalent volumes of DMSO (Sigma Aldrich,  
322 St. Louis, MO) served as a negative control. For DMSO-treated and mitotically arrested  
323 populations of MCF10A cells, harvests were conducted following the 16hr incubation. For  
324 G1 (released from mitotic arrest) populations of MCF10A cells, the nocodazole-  
325 supplemented culturing media was replaced with normal culturing media and incubated  
326 with cells for 3hrs. Following the 3hr incubation, released populations of cells were  
327 harvested for subsequent analysis.

328 **Protein Expression and Localization**

329 SDS-PAGE was performed to visualize protein expression within MCF10A cells.  
330 8% SDS resolving gels and 4% stacking gels were prepared in-house (National  
331 Diagnostics, Atlanta, GA). Cell harvests were resuspended in RIPA buffer and incubated  
332 on ice for 30min. Following incubation, cell lysates were sonicated using Q700 Sonicator

333 (QSonica, Newtown, CT). Total sonication time for samples were 70 seconds, with 7  
334 programed cycles of 10 seconds sonication at power setting 30 followed by 30 seconds  
335 of no sonication. Sonicated lysates were centrifuged at 15,000 rpm for 30min at 4°C.  
336 Protein concentration in the remaining supernatant was quantified using a Pierce™ BCA  
337 Protein Assay Kit (Thermo Fisher Scientific, Ashville, NC). Electrophoresis was performed  
338 at 160V for 15min followed by 200V for 45min. Overnight wet transfer of protein into PVDF  
339 membranes was performed at 30V for 18hr in 4°C. PVDF membranes were blocked at  
340 room temperature in 5% BSA in 1X TBST. Primary antibodies used for protein  
341 visualization were diluted 1:1000 and raised against UBF (sc-13125, Santa Cruz  
342 Biotechnology, Dallas, TX), RUNX1 (4334S, Cell Signaling Technologies, Danvers, MA),  
343 Cyclin B (4138S, Cell Signaling Technologies, Danvers, MA), Beta-Actin (3700S, Cell  
344 Signaling Technologies, Danvers, MA), and CDT1 (ab70829, AbCam, Cambridge, UK).  
345 Lamin B1 (ab16048, AbCam, Cambridge, UK) primary antibody was used at 1:2000  
346 dilution for protein visualization. Primary antibodies were diluted in 5% BSA in 1XTBST  
347 and incubated with blots overnight at 4°C. Blots were washed four separate times with  
348 PBST or TBST. Goat anti-mouse IgG HRP conjugated (31460, Invitrogen, Carlsbad, CA)  
349 secondary antibody was incubated with blots at 1:5000 and incubated for 1hr at room  
350 temperature with mild agitation. Goat anti-rabbit IgG HRP conjugated (31430, Thermo  
351 Fisher Scientific, Ashville, NC) secondary antibody was incubated with blots at 1:1000,  
352 1:2000, or 1:5000 and incubated for 1hr at room temperature with mild agitation. Blots  
353 were developed using Clarity Western ECL Substrate (Bio-Rad, Hercules, CA) following  
354 manufacturer's instructions. Blots were exposed to visualize protein and images were  
355 captured using Molecular Imager® Chemi doc™ XRS+ Imaging System (Bio-Rad,

356 Hercules, CA). Captured images were processed using Image Lab Software Version 5.1  
357 (Bio-Rad, Hercules, CA).

358 Immunofluorescent microscopy was performed to observe distribution and  
359 localization of protein expression within MCF10A cells throughout all stages of mitosis  
360 and interphase. MCF10A cells were plated within a 6 well plate at 175,000 cells/mL on  
361 coverslips coated in gelatin (0.5% w/v solution in 1XPBS) and allowed to grow overnight.  
362 Coverslips were washed twice with sterile-filtered PBS at 4°C. Coverslips were then  
363 placed in room temperature fixative solution (1% MeOH-free Formaldehyde in PBS) for  
364 10min. After a sterile-filtered PBS wash, coverslips were transferred to permeabilization  
365 solution (0.25% Triton X-100 in PBS) for 20min on ice. Following another sterile-filtered  
366 PBS wash, coverslips were then blocked in sterile-filtered PBS supplemented with bovine  
367 serum albumin (PBSA) at 0.5% w/v (Sigma Aldrich, St. Louis, MO). Coverslips were then  
368 incubated with primary antibody for 1hr at 37°C in a humidified chamber. Primary  
369 antibodies were specific for RUNX1 at a dilution of 1:10 (4334S, Cell Signaling  
370 Technologies, Danvers, MA) and Upstream Binding Transcription Factor (UBF) at a  
371 dilution of 1:200 (F-9 sc-13125, Santa Cruz Biotechnology, Dallas, TX). Coverslips were  
372 washed four separate times in sterile-filtered PBSA following primary antibody incubation.  
373 Coverslips were then placed in secondary antibody for 1hr at 37°C within a humidified  
374 chamber. Secondary antibodies used were goat anti-rabbit IgG conjugated with Alexa  
375 Fluor 488 (A-11070, Life Technologies, Carlsbad, CA) and goat anti-mouse IgG  
376 conjugated with Alexa Fluor 594 (A-11005, Life Technologies, Carlsbad, CA) diluted  
377 1:800. Coverslips were then washed four times in sterile-filtered PBSA. Staining of the  
378 coverslips for DNA was performed with 1.0µg DAPI in 0.1% Triton X-100 and sterile-

379 filtered PBSA for 5min on ice. Stained coverslips were washed once in 0.1% Triton X-100  
380 in sterile-filtered PBSA, then two times with sterile filtered PBS. Coverslips were mounted  
381 onto slides using ProLong Gold Antifade Mountant (Thermo Fisher Scientific, Ashville,  
382 NC). Images were captured using a Zeiss Axio Imager.Z2 fluorescent microscope and  
383 Hamamatsu ORCA-R<sup>2</sup> C10600 digital camera. Images were processed using ZEN 2012  
384 software.

385 Confocal microscopy was performed on slides prepared as described above.  
386 MCF10A breast epithelial cells were initially imaged with a Zeiss LSM 510 META confocal  
387 laser scanning microscope (Carl Zeiss Microscopy, LLC., Thornwood, NY, USA) for a  
388 preliminary study to assess potential colocalization. At a later time, additional samples  
389 were imaged with a Nikon A1R-ER laser scanning confocal microscope (Nikon, Melville,  
390 NY, USA) for complete colocalization analysis. Images were acquired with the resonant  
391 scanner at a frame size of 1024 X 1024 pixels with 8X averaging. Fluorescently labeled  
392 samples were excited by laser lines sequentially imaged in channel series mode. The  
393 DAPI signal was excited with a 405 nm laser and collected with a 425-475 nm band pass  
394 filter, Alexa 488 was excited with a 488 nm laser and collected with a 500-550 nm band  
395 pass filter, and Alexa 568 with a 561 nm laser and collected with a 570-620 nm band pass  
396 filter. Images were captured with a Plan-Fluor 40X (1.3 NA) objective lens. The confocal  
397 pinhole was initially set to 1.2 Airy Unit diameter for the 561 nm excitation giving an optical  
398 section thickness of 0.41 μm. Images were acquired at 12-bit data depth, and all settings,  
399 including laser power, amplifier gain, and amplifier offset were established using a look-  
400 up table to provide an optimal gray-scale intensities. All images were acquired using  
401 matching imaging parameters.

402        Images were acquired with at 40X objective were subject to colocalization analysis  
403        via Volocity version 6.3.0 (Perkin Elmer, Waltham, MA, USA). Images were opened in  
404        the colocalization tab. Cell nuclei, indicated by the DAPI signal, were circled via the ROI  
405        tool. At least 15 interphase and 15 metaphase cells were identified within captured  
406        images and appropriate thresholds were manually determined to eliminate background  
407        fluorescence for calculating Pearsons and Manders correlation coefficients between  
408        RUNX1 and UBF.

409        Images were also viewed in NIS Elements version 5.02.01 and analyzed using the  
410        line profiling tool. Overlaying DAPI, RUNX1, and UBF fluorescent intensities from  
411        individual channels along the line profile revealed overlapping peak intensities between  
412        the RUNX1 and UBF channels, thus indicating colocalization.

413        Core binding factor – Beta (CBF $\beta$ ) inhibitors AI-4-88 and AI-14-91 were given to  
414        us from John H. Bushweller (University of Virginia) and used to evaluate RUNX1 DNA-  
415        binding inhibition in MCF10A cells. Protein synthesis evaluation by immunofluorescence  
416        was conducted following manufacturer protocol (K715-100, BioVision, San Francisco,  
417        CA).

418        **Molecular Techniques**

419        Total RNA was isolated from MCF10A cells using TRIzol<sup>TM</sup> Reagent (Invitrogen,  
420        Carlsbad, CA) and Direct-Zol<sup>TM</sup> RNA MiniPrep isolation kit (Zymo Research, Irvine, CA)  
421        following manufacturer instructions. cDNA was created using SuperScript IV<sup>®</sup> First-  
422        Strand Synthesis System for RT-PCR (ThermoFisher, Asheville, NC). Resulting samples  
423        were quantified on a Qubit 2.0 Fluorometer (Invitrogen, Carlsbad, CA) and diluted to  
424        500pg/ $\mu$ L. Equal amounts of DNA template were loaded for samples analyzed by qPCR.

425 Chromatin Immunoprecipitation was conducted on asynchronous (Asynch),  
426 mitotically arrested (M), and released from mitosis (G1) MCF10A breast epithelial cells.  
427 Cells were fixed with 1% v/v MeOH-free Formaldehyde in 1XPBS for 10min at room  
428 temperature. Formaldehyde fixation was neutralized using 2.5M Glycine and incubated  
429 with cells for 5min at room temperature. Two washes with 1XPBS supplemented with  
430 cComplete™ EDTA-free Protease Inhibitor Cocktail (Sigma Aldrich, Saint Louis, MO) and  
431 MG-132 (Calbiochem-Millipore Sigma, Burlington, MA) were performed. For  
432 asynchronous and G1 populations of cells, culture dishes were scraped to collect fixated  
433 lysate. Mitotic cells were isolated using a mitotic shake off. Mitotic cells were spun down  
434 at 1500rpm x 5min, resuspended in 1% v/v MeOH-free Formaldehyde in 1XPBS, and  
435 neutralized with 2.5M Glycine for 5min. Fixed harvests were centrifuged at 1500rpm x  
436 5min (4°C) and the supernatant was discarded. All fixed cell pellets were flash frozen in  
437 liquid nitrogen and stored at -80°C until lysis.

438 Fixed cell pellets were thawed on ice. Once thawed, pellets were lysed in a nuclear  
439 lysis buffer supplemented with cComplete™ EDTA-free Protease Inhibitor Cocktail (Sigma  
440 Aldrich, Saint Louis, MO) and MG-132 (Calbiochem-Millipore Sigma, Burlington, MA) with  
441 a volume that was approximately 5X the volume of pellet. Pellets were incubated in  
442 nuclear lysis buffer for 30min before being flash frozen down in liquid nitrogen. Lysates  
443 were thawed at room temperature but not allowed to reach room temperature. Sonication  
444 of the lysates were performed using a S220 focused ultra-sonicator (Covaris, Matthews,  
445 NC). Sonication parameters for each population of cells was as follows: Peak Watt 140W,  
446 Duty Factor 10, Cycle/Burst 200. M and G1 populations of cells were sonicated for 28min  
447 total whereas asynchronous populations of cells were sonicated for 36min. All samples

448 were sonicated at 6°C. Following sonication, aliquots were spun down at 15,000rpm x  
449 10min and 4°C. Following the spin, the resulting supernatants were pooled together and  
450 analyzed.

451 Sonicated lysate was boiled in 100°C for 15min with NaCl and elution buffer. Boiled  
452 lysate was allowed to cool and treated with RNaseA (10ug/uL) for 10min at 37°C. DNA  
453 was isolated using PureLink™ PCR Purification Kit (K310001, ThermoFisher, Ashville,  
454 NC) following manufacturer recommendations. Resulting DNA was quantified via  
455 nanodrop and 1.0-2.0ug was run on a 1.5% agarose gel to observe sonication results  
456 prior to generating ChIP reactions. Resulting DNA was also quantified via Qubit 2.0  
457 Fluorometer (Invitrogen, Carlsbad, CA) and analyzed by using a High Sensitivity DNA Kit  
458 on a Bioanalyzer 2100 (Agilent, Santa Clara, CA).

459 For chromatin immunoprecipitation (ChIP) reactions, 150ug of sonicated  
460 chromatin was incubated with 10ug of RUNX1 antibody (4336BF, Cell Signaling  
461 Technologies, Danvers, MA), diluted 1:10 in IP dilution buffer, and incubated overnight  
462 (16-18hrs) at 4°C with mild agitation. Following incubation, 150uL of Protein A/G magnetic  
463 beads (Thermo Scientific – Pierce, Waltham, MA) per ug of antibody used were added to  
464 each IP reaction and incubated for 2-4hrs at 4°C with mild agitation. Beads were isolated  
465 from solution using a powerful magnet, and washed two times in two separate IP wash  
466 buffers. Lastly, beads were resuspended in an elution buffer and agitated in a  
467 thermomixer (Eppendorf, Hamburg, Germany) or vortexer at 1000rpm x 30min at room  
468 temperature. This elution step was repeated on the beads. Using a magnet, beads were  
469 discarded and the resulting supernatant was incubated with NaCl overnight (16-18hrs) at  
470 67°C to reverse formaldehyde crosslinks. DNA from RUNX1 ChIP samples were purified

471 using PureLink™ PCR Purification Kit (K310001, ThermoFisher, Ashville, NC) following  
472 manufacturer recommendations.

473 ChIP libraries were generated using Accel-NGS® 2S Plus DNA Library kit (Swift  
474 Biosciences, Ann Arbor, MI) following manufacturers protocol. Input and RUNX1 ChIP  
475 samples were normalized to 1ng prior to library generation. Libraries were amplified in an  
476 optional PCR step for 12 total cycles. Finalized libraries were double size selected using  
477 AMPure XP beads (0.8X and 0.2X volume ratios to sample), resulting in the majority  
478 fragments sized between 250-400bp. Next generation sequencing of pooled ChIP  
479 libraries was performed by the University of Vermont Cancer Center - Vermont Integrated  
480 Genomics Resource (VIGR).

481

## 482 **Bioinformatics Analyses**

483 Because we were specifically investigating rDNA, a customized build of hg38 was  
484 constructed that included normally masked regions of rDNA (Gencode U13369). Since  
485 some (although not complete) rDNA sequence is present in the hg38 assembly, we  
486 masked all parts of hg38 that would normally be attributed to rDNA sequences (bedtools  
487 v2.25.0 maskfasta). Finally, we appended the complete rDNA sequence as a “unique”  
488 chromosome (chrU13369.1) to the masked hg38 FASTA resulting in the hg38\_rDNA  
489 assembly used for analysis.

490 Single-end, 50bp reads (SE50) were processed pre-alignment by removing adapter reads  
491 (Cutadapt v1.6) and trimming low quality base calls from both ends (FASTQ Quality  
492 Trimmer 1.0.0; min score >= 20, window of 10, and step size of 1). Resulting reads were  
493 aligned to hg38\_rDNA (STAR v2.4; splicing disabled with '--alignIntronMax 1'). Next, we

494 called peaks and generated fold-enrichment (FE) bedGraph files (MACS2  
495 v2.1.0.20140616; callpeak at p-value e-5; and bdgcmp with FE method)<sup>63</sup>. Irreproducible  
496 Discovery Rate (IDR) was conducted using unpooled replicates with all peaks in pooled  
497 samples passing an IDR cutoff of 0.5<sup>64</sup>. To reduce artificial peaks, we calculated strand  
498 cross-correlation for all peaks at a shift of 95 bp (the mean observed fragment size of 180  
499 bp minus the read size of 85bp) and unshifted<sup>65</sup>. We eliminated peaks that exhibited low  
500 shifted correlation (shifted correlation <.7) and those that exhibited high unshifted  
501 correlation relative to shifted (shifted – unshifted correlation < .1). This increased retrieval  
502 of the RUNX1 motif and improved agreement with other RUNX1 datasets. Passing peaks  
503 were annotated separately to mRNA and lncRNA transcript start sites (TSSs) using  
504 GENCODE v27 with a distance cutoff of 5000 bp. Regional distribution of peaks was  
505 determined using the same annotation reference limited to the “basic” tag for exons and  
506 promoters.

507

## 508 **ACKNOWLEDGEMENTS**

509 The authors would like to thank John H. Bushweller, PhD (University of Virginia),  
510 who created and gifted us Core binding factor – Beta (CBFβ) inhibitors AI-4-88 and AI-  
511 14-91 to conduct RUNX1 inhibition experiments for this study. Confocal imaging and  
512 colocalization analysis were performed by Nicole Bouffard in the Microscopy Imaging  
513 Center at the University of Vermont College of Medicine. The authors would also like to  
514 thank Scott Tighe, Pheobe Kehoe, and Jessica Hoffman for performing next generation  
515 sequencing of samples (Vermont Integrated Genomics Resource (VIGR) at the University  
516 of Vermont Cancer Center). The authors also thank Roxana del Rio-Guerra, Ph.D of the

517 UVM Flow Cytometry and Cell Sorting Facility for analysis of samples by FACS. The  
518 authors would also like to thank Alan Howe, Ph.D. (University of Vermont) for his  
519 Phalloidin reagent used in immunofluorescence microscopy experiments.

520

521 **COMPETING INTERESTS**

522 No competing interests declared.

523

524 **FUNDING**

525 This work was supported by NIH grants NCI P01 CA082834 (to G.S. Stein and J.L.  
526 Stein), R01 CA139322 (to G.S. Stein), R37 DE012528 (to J.B. Lian), NCI F32 CA220935  
527 (to A.J. Fritz, G.S. Stein, and J.L. Stein), U01 CA196383 (to J.L. Stein), and the Charlotte  
528 Perelman Fund for Cancer Research (to G.S. Stein). The confocal microscopy work  
529 described in this manuscript was supported by Award Number 1S10RR019246 from the  
530 National Center for Research Resources for purchase of the Zeiss 510 META confocal  
531 scanning laser microscope and NIH award number 1S10OD025030-01 for purchase of  
532 the Nikon A1R-ER point scanning confocal microscope from the National Center for  
533 Research Resources. FACS experiments performed at the Harry Hood Bassett Flow  
534 Cytometry and Cell Sorting Facility, University of Vermont College of Medicine were  
535 supported by NIH S10-ODO18175.

536

537 **DATA AVAILABILITY**

538 GEO accession number for the sequencing data generated in this study is  
539 GSE121370.

540 REFERENCES

- 541 1 Hanahan, D. & Weinberg, R. A. Hallmarks of cancer: the next generation. *Cell* **144**, 646-  
542 674, doi:10.1016/j.cell.2011.02.013 (2011).
- 543 2 Micalizzi, D. S., Farabaugh, S. M. & Ford, H. L. Epithelial-mesenchymal transition in  
544 cancer: parallels between normal development and tumor progression. *Journal of  
545 mammary gland biology and neoplasia* **15**, 117-134, doi:10.1007/s10911-010-9178-9  
546 (2010).
- 547 3 Schmalhofer, O., Brabletz, S. & Brabletz, T. E-cadherin, beta-catenin, and ZEB1 in  
548 malignant progression of cancer. *Cancer metastasis reviews* **28**, 151-166,  
549 doi:10.1007/s10555-008-9179-y (2009).
- 550 4 Taube, J. H. et al. Core epithelial-to-mesenchymal transition interactome gene-expression  
551 signature is associated with claudin-low and metaplastic breast cancer subtypes. *Proc Natl  
552 Acad Sci U S A* **107**, 15449-15454, doi:10.1073/pnas.1004900107 (2010).
- 553 5 Yang, J. & Weinberg, R. A. Epithelial-mesenchymal transition: at the crossroads of  
554 development and tumor metastasis. *Developmental cell* **14**, 818-829,  
555 doi:10.1016/j.devcel.2008.05.009 (2008).
- 556 6 Dowdy, C. R. et al. Definitive hematopoiesis requires Runx1 C-terminal-mediated  
557 subnuclear targeting and transactivation. *Hum Mol Genet* **19**, 1048-1057,  
558 doi:10.1093/hmg/ddp568 (2010).
- 559 7 Hilton, M. J. et al. Notch signaling maintains bone marrow mesenchymal progenitors by  
560 suppressing osteoblast differentiation. *Nature medicine* **14**, 306-314, doi:10.1038/nm1716  
561 (2008).
- 562 8 Huang, H. et al. A Src family kinase-Shp2 axis controls RUNX1 activity in megakaryocyte  
563 and T-lymphocyte differentiation. *Genes & development* **26**, 1587-1601,  
564 doi:10.1101/gad.192054.112 (2012).
- 565 9 Ito, K. et al. RUNX3 attenuates beta-catenin/T cell factors in intestinal tumorigenesis.  
566 *Cancer cell* **14**, 226-237, doi:10.1016/j.ccr.2008.08.004 (2008).
- 567 10 Ito, Y. RUNX genes in development and cancer: regulation of viral gene expression and  
568 the discovery of RUNX family genes. *Advances in cancer research* **99**, 33-76,  
569 doi:10.1016/s0065-230x(07)99002-8 (2008).
- 570 11 Ito, Y., Bae, S. C. & Chuang, L. S. The RUNX family: developmental regulators in cancer.  
571 *Nat Rev Cancer* **15**, 81-95, doi:10.1038/nrc3877 (2015).
- 572 12 Ito, Y. & Miyazono, K. RUNX transcription factors as key targets of TGF-beta superfamily  
573 signaling. *Current opinion in genetics & development* **13**, 43-47 (2003).
- 574 13 Lam, K. & Zhang, D. E. RUNX1 and RUNX1-ETO: roles in hematopoiesis and  
575 leukemogenesis. *Frontiers in bioscience (Landmark edition)* **17**, 1120-1139 (2012).
- 576 14 Min, B. et al. Identification of RUNX3 as a component of the MST/Hpo signaling pathway.  
577 *Journal of cellular physiology* **227**, 839-849, doi:10.1002/jcp.22887 (2012).
- 578 15 Pratap, J. et al. Runx2 transcriptional activation of Indian Hedgehog and a downstream  
579 bone metastatic pathway in breast cancer cells. *Cancer Res* **68**, 7795-7802,  
580 doi:10.1158/0008-5472.CAN-08-1078 (2008).
- 581 16 Tai, P. W. L. et al. Genome-wide DNase hypersensitivity, and occupancy of RUNX2 and  
582 CTCF reveal a highly dynamic gene regulome during MC3T3 pre-osteoblast  
583 differentiation. *PloS one* **12**, e0188056, doi:10.1371/journal.pone.0188056 (2017).
- 584 17 VanOudenhoove, J. J. et al. Transient RUNX1 Expression during Early Mesendodermal  
585 Differentiation of hESCs Promotes Epithelial to Mesenchymal Transition through TGFB2  
586 Signaling. *Stem Cell Reports* **7**, 884-896, doi:10.1016/j.stemcr.2016.09.006 (2016).

- 587 18 Vega, O. A. *et al.* Wnt/beta-Catenin Signaling Activates Expression of the Bone-Related  
588 Transcription Factor RUNX2 in Select Human Osteosarcoma Cell Types. *Journal of*  
589 *cellular biochemistry* **118**, 3662-3674, doi:10.1002/jcb.26011 (2017).
- 590 19 Zheng, L. *et al.* Runx2/DICER/miRNA Pathway in Regulating Osteogenesis. *Journal of*  
591 *cellular physiology* **232**, 182-191, doi:10.1002/jcp.25406 (2017).
- 592 20 Browne, G. *et al.* MicroRNA-378-mediated suppression of Runx1 alleviates the aggressive  
593 phenotype of triple-negative MDA-MB-231 human breast cancer cells. *Tumour Biol* **37**,  
594 8825-8839, doi:10.1007/s13277-015-4710-6 (2016).
- 595 21 Browne, G. *et al.* Runx1 is associated with breast cancer progression in MMTV-PyMT  
596 transgenic mice and its depletion in vitro inhibits migration and invasion. *J Cell Physiol*  
597 **230**, 2522-2532, doi:10.1002/jcp.24989 (2015).
- 598 22 Chimge, N. O. *et al.* RUNX1 prevents oestrogen-mediated AXIN1 suppression and beta-  
599 catenin activation in ER-positive breast cancer. *Nature communications* **7**, 10751,  
600 doi:10.1038/ncomms10751 (2016).
- 601 23 Hong, D. *et al.* Runx1 stabilizes the mammary epithelial cell phenotype and prevents  
602 epithelial to mesenchymal transition. *Oncotarget* **8**, 17610-17627,  
603 doi:10.18632/oncotarget.15381 (2017).
- 604 24 Recouvreux, M. S. *et al.* RUNX1 and FOXP3 interplay regulates expression of breast  
605 cancer related genes. *Oncotarget* **7**, 6552-6565, doi:10.18632/oncotarget.6771 (2016).
- 606 25 Comprehensive molecular portraits of human breast tumours. *Nature* **490**, 61-70,  
607 doi:10.1038/nature11412 (2012).
- 608 26 Banerji, S. *et al.* Sequence analysis of mutations and translocations across breast cancer  
609 subtypes. *Nature* **486**, 405-409, doi:10.1038/nature11154 (2012).
- 610 27 Ellis, M. J. *et al.* Whole-genome analysis informs breast cancer response to aromatase  
611 inhibition. *Nature* **486**, 353-360, doi:10.1038/nature11143 (2012).
- 612 28 Liu, Y. N. *et al.* Regulatory mechanisms controlling human E-cadherin gene expression.  
613 *Oncogene* **24**, 8277-8290, doi:10.1038/sj.onc.1208991 (2005).
- 614 29 John, S. & Workman, J. L. Bookmarking genes for activation in condensed mitotic  
615 chromosomes. *Bioessays* **20**, 275-279, doi:10.1002/(SICI)1521-  
616 1878(199804)20:4<275::AID-BIES1>3.0.CO;2-P (1998).
- 617 30 Raccaud, M. & Suter, D. M. Transcription factor retention on mitotic chromosomes:  
618 regulatory mechanisms and impact on cell fate decisions. *FEBS letters* **592**, 878-887,  
619 doi:10.1002/1873-3468.12828 (2018).
- 620 31 Sarge, K. D. & Park-Sarge, O. K. Gene bookmarking: keeping the pages open. *Trends*  
621 *Biochem Sci* **30**, 605-610, doi:10.1016/j.tibs.2005.09.004 (2005).
- 622 32 Caravaca, J. M. *et al.* Bookmarking by specific and nonspecific binding of FoxA1 pioneer  
623 factor to mitotic chromosomes. *Genes Dev* **27**, 251-260, doi:10.1101/gad.206458.112  
624 (2013).
- 625 33 Deluz, C. *et al.* A role for mitotic bookmarking of SOX2 in pluripotency and differentiation.  
626 *Genes & development* **30**, 2538-2550, doi:10.1101/gad.289256.116 (2016).
- 627 34 Kadouke, S. *et al.* Tissue-specific mitotic bookmarking by hematopoietic transcription  
628 factor GATA1. *Cell* **150**, 725-737, doi:10.1016/j.cell.2012.06.038 (2012).
- 629 35 Lake, R. J., Tsai, P. F., Choi, I., Won, K. J. & Fan, H. Y. RBPJ, the major transcriptional  
630 effector of Notch signaling, remains associated with chromatin throughout mitosis,  
631 suggesting a role in mitotic bookmarking. *PLoS Genet* **10**, e1004204,  
632 doi:10.1371/journal.pgen.1004204 (2014).
- 633 36 Liu, Y. *et al.* Widespread Mitotic Bookmarking by Histone Marks and Transcription Factors  
634 in Pluripotent Stem Cells. *Cell Rep* **19**, 1283-1293, doi:10.1016/j.celrep.2017.04.067  
635 (2017).
- 636 37 Ali, S. A. *et al.* Phenotypic transcription factors epigenetically mediate cell growth control.  
637 *Proc Natl Acad Sci U S A* **105**, 6632-6637, doi:10.1073/pnas.0800970105 (2008).

- 638 38 Young, D. W. *et al.* Mitotic occupancy and lineage-specific transcriptional control of rRNA  
639 genes by Runx2. *Nature* **445**, 442-446, doi:10.1038/nature05473 (2007).  
640 39 Young, D. W. *et al.* Mitotic retention of gene expression patterns by the cell fate-  
641 determining transcription factor Runx2. *Proc Natl Acad Sci U S A* **104**, 3189-3194,  
642 doi:10.1073/pnas.0611419104 (2007).  
643 40 Zaidi, S. K. *et al.* Mitotic partitioning and selective reorganization of tissue-specific  
644 transcription factors in progeny cells. *Proceedings of the National Academy of Sciences of  
645 the United States of America* **100**, 14852-14857, doi:10.1073/pnas.2533076100 (2003).  
646 41 Shrivastava, T. *et al.* Structural basis of Ets1 activation by Runx1. *Leukemia* **28**, 2040-  
647 2048, doi:10.1038/leu.2014.111 (2014).  
648 42 Carlton, A. L. *et al.* Small molecule inhibition of the CBFbeta/RUNX interaction decreases  
649 ovarian cancer growth and migration through alterations in genes related to epithelial-to-  
650 mesenchymal transition. *Gynecol Oncol* **149**, 350-360, doi:10.1016/j.ygyno.2018.03.005  
651 (2018).  
652 43 Illendula, A. *et al.* Small Molecule Inhibitor of CBFbeta-RUNX Binding for RUNX  
653 Transcription Factor Driven Cancers. *EBioMedicine* **8**, 117-131,  
654 doi:10.1016/j.ebiom.2016.04.032 (2016).  
655 44 Kim, W. *et al.* RUNX1 is essential for mesenchymal stem cell proliferation and  
656 myofibroblast differentiation. *Proc Natl Acad Sci U S A* **111**, 16389-16394,  
657 doi:10.1073/pnas.1407097111 (2014).  
658 45 Ozaki, T., Nakagawara, A. & Nagase, H. RUNX Family Participates in the Regulation of  
659 p53-Dependent DNA Damage Response. *International journal of genomics* **2013**, 271347,  
660 doi:10.1155/2013/271347 (2013).  
661 46 Satoh, Y. *et al.* C-terminal mutation of RUNX1 attenuates the DNA-damage repair  
662 response in hematopoietic stem cells. *Leukemia* **26**, 303-311, doi:10.1038/leu.2011.202  
663 (2012).  
664 47 Wang, C. Q. *et al.* Disruption of Runx1 and Runx3 leads to bone marrow failure and  
665 leukemia predisposition due to transcriptional and DNA repair defects. *Cell Rep* **8**, 767-  
666 782, doi:10.1016/j.celrep.2014.06.046 (2014).  
667 48 Wu, D., Ozaki, T., Yoshihara, Y., Kubo, N. & Nakagawara, A. Runt-related transcription  
668 factor 1 (RUNX1) stimulates tumor suppressor p53 protein in response to DNA damage  
669 through complex formation and acetylation. *The Journal of biological chemistry* **288**, 1353-  
670 1364, doi:10.1074/jbc.M112.402594 (2013).  
671 49 Cargnello, M., Tcherkezian, J. & Roux, P. P. The expanding role of mTOR in cancer cell  
672 growth and proliferation. *Mutagenesis* **30**, 169-176, doi:10.1093/mutage/geu045 (2015).  
673 50 Ciruelos Gil, E. M. Targeting the PI3K/AKT/mTOR pathway in estrogen receptor-positive  
674 breast cancer. *Cancer treatment reviews* **40**, 862-871, doi:10.1016/j.ctrv.2014.03.004  
675 (2014).  
676 51 Feng, Y., Manka, D., Wagner, K. U. & Khan, S. A. Estrogen receptor-alpha expression in  
677 the mammary epithelium is required for ductal and alveolar morphogenesis in mice. *Proc  
678 Natl Acad Sci U S A* **104**, 14718-14723, doi:10.1073/pnas.0706933104 (2007).  
679 52 Mallepell, S., Krust, A., Chambon, P. & Brisken, C. Paracrine signaling through the  
680 epithelial estrogen receptor alpha is required for proliferation and morphogenesis in the  
681 mammary gland. *Proc Natl Acad Sci U S A* **103**, 2196-2201,  
682 doi:10.1073/pnas.0510974103 (2006).  
683 53 Mueller, S. O., Clark, J. A., Myers, P. H. & Korach, K. S. Mammary gland development in  
684 adult mice requires epithelial and stromal estrogen receptor alpha. *Endocrinology* **143**,  
685 2357-2365, doi:10.1210/endo.143.6.8836 (2002).  
686 54 Stender, J. D. *et al.* Genome-wide analysis of estrogen receptor alpha DNA binding and  
687 tethering mechanisms identifies Runx1 as a novel tethering factor in receptor-mediated  
688 transcriptional activation. *Mol Cell Biol* **30**, 3943-3955, doi:10.1128/MCB.00118-10 (2010).

- 689 55 Gutschner, T., Hammerle, M. & Diederichs, S. MALAT1 -- a paradigm for long noncoding  
690 RNA function in cancer. *Journal of molecular medicine (Berlin, Germany)* **91**, 791-801,  
691 doi:10.1007/s00109-013-1028-y (2013).
- 692 56 Yu, X., Li, Z., Zheng, H., Chan, M. T. & Wu, W. K. NEAT1: A novel cancer-related long  
693 non-coding RNA. *Cell Prolif* **50**, doi:10.1111/cpr.12329 (2017).
- 694 57 Li, X., Cao, Y., Li, M. & Jin, F. Upregulation of HES1 Promotes Cell Proliferation and  
695 Invasion in Breast Cancer as a Prognosis Marker and Therapy Target via the AKT  
696 Pathway and EMT Process. *Journal of Cancer* **9**, 757-766, doi:10.7150/jca.22319 (2018).
- 697 58 Strom, A., Arai, N., Leers, J. & Gustafsson, J. A. The Hairy and Enhancer of Split  
698 homologue-1 (HES-1) mediates the proliferative effect of 17beta-estradiol on breast  
699 cancer cell lines. *Oncogene* **19**, 5951-5953 (2000).
- 700 59 Weyemi, U. *et al.* Twist1 and Slug mediate H2AX-regulated epithelial-mesenchymal  
701 transition in breast cells. *Cell cycle (Georgetown, Tex.)* **15**, 2398-2404,  
702 doi:10.1080/15384101.2016.1198864 (2016).
- 703 60 Kageyama, R., Ohtsuka, T. & Kobayashi, T. The Hes gene family: repressors and  
704 oscillators that orchestrate embryogenesis. *Development (Cambridge, England)* **134**,  
705 1243-1251, doi:10.1242/dev.000786 (2007).
- 706 61 Rani, A., Greenlaw, R., Smith, R. A. & Galustian, C. HES1 in immunity and cancer.  
707 *Cytokine & growth factor reviews* **30**, 113-117, doi:10.1016/j.cytofr.2016.03.010 (2016).
- 708 62 Barutcu, A. R. *et al.* RUNX1 contributes to higher-order chromatin organization and gene  
709 regulation in breast cancer cells. *Biochim Biophys Acta* **1859**, 1389-1397,  
710 doi:10.1016/j.bbapm.2016.08.003 (2016).
- 711 63 Zhang, Y. *et al.* Model-based analysis of ChIP-Seq (MACS). *Genome Biol* **9**, R137,  
712 doi:10.1186/gb-2008-9-9-r137 (2008).
- 713 64 Li, Q., Brown, J. B., Huang, H. & Bickel, P. J. Measuring reproducibility of high-throughput  
714 experiments.
- 715 65 Landt, S. G. *et al.* ChIP-seq guidelines and practices of the ENCODE and modENCODE  
716 consortia. *Genome research* **22**, 1813-1831, doi:10.1101/gr.136184.111 (2012).

717

718 **FIGURE LEGENDS**

719 **Figure 1. RUNX1 associates with DNA during interphase and remains bound**  
720 **throughout mitosis in the form of major and minor foci.** Representative  
721 immunofluorescent images of interphase and mitotic MCF10A breast epithelial cells.  
722 Mitotic cells were further classified into substages of mitosis based on DAPI topology.  
723 RUNX1 – Green (top row), DAPI – Blue (second row from top). Merged channel images  
724 (third row from top) contain an outlined region magnified in the bottom row labeled  
725 “inset”. White arrows highlight major Runx1 foci on chromatin.

726

727 **Figure 2. RUNX1 occupies protein coding genes and long non-coding RNAs**  
728 **across asynchronous, mitotic, and G1 populations of MCF10A breast epithelial**  
729 **cells.** A) Experimental schematic depicting mitotic arrest and harvest of each treated  
730 MCF10A cell populations: Asynchronous – A, Mitotic – M, and Released – G1. B)  
731 Western blot of each harvested MCF10A population for cell cycle specific markers to  
732 evaluate mitotic arrest and synchronization procedure. C) Fluorescently activated cell  
733 sorting (FACS) analysis of harvested A, M, and G1 MCF10A cells to determine mitotic  
734 purity and DNA content (n=3 biological replicates per group). D) Heatmaps showing  
735 peaks called between A, M, and G1 MCF10A cells (left, middle, and right respectively).  
736 E) Venn diagrams illustrating the number of protein coding genes (left diagram) and  
737 lncRNAs (right diagram) identified within and between A, M, and G1 MCF10A  
738 populations. F) Motif analysis of A, M, and G1 MCF10A cells

739

740 **Figure 3. RUNX1 colocalizes with RNA Pol I subunit, upstream binding factor**  
741 **(UBF) on mitotic chromatin.** A) Immunofluorescence microscopy images of RUNX1  
742 (green – top row), UBF (red – 2<sup>nd</sup> row from top), DAPI (blue – 2<sup>nd</sup> row from bottom), and  
743 the three channels merged (bottom row) in MCF10A cells. Images were captured of  
744 spontaneously dividing MCF10A cells in different substages of mitosis. B)  
745 Representative images of line profiles taken on interphase vs metaphase cells (n=15  
746 each).

747

748 **Figure 4. RUNX1 bookmarks rDNA promoter repeat regions and affects both pre-**  
749 **rRNA and global protein expression.** A) ChIP-Seq tracks of A, M, and G1 (top,  
750 middle, bottom respectively) MCF10A cells mapped against rDNA repeat regions. B)  
751 Representative immunofluorescence images of the active compound (AI-14-91)-treated  
752 MCF10A cells in prophase and metaphase are shown. A substantial decrease in  
753 smaller RUNX1 foci (green) during mitosis is observed when compared to the inactive  
754 (AI-4-88) compound. Large RUNX1 foci that colocalize with UBF (red) are detectable at  
755 all substages of mitosis (white arrows) in the presence of either active or inactive  
756 compounds. C) qRT-PCR data of pre-rRNA in actively proliferating MCF10A cells  
757 treated with either active (AI-14-91) or inactive (AI-4-88) compounds for 6, 12, 24, or  
758 48hrs. Expression of pre-rRNA was normalized relative to Beta Actin expression. D)  
759 Representative fluorescence microscopy images of global protein synthesis occurring  
760 within MCF10A cells treated with either AI-4-88 (left) or AI-14-91 (right) for 24hr at  
761 20 $\mu$ M. Intensity of red fluorescence at 580nm emission indicates nascent protein  
762 synthesis. All images were taken with 1000ms exposures.

763

764 **Figure 5. RUNX1 bookmarks RNA Pol II-transcribed genes involved in**  
765 **maintenance of breast epithelial phenotype.** A) Gene Set Enrichment (GSE) analysis  
766 from interrogating mitotically bookmarked genes (i.e. RUNX1 mitotically occupied)  
767 against Hallmark Gene sets from Molecular Signatures Database (MSigDB). The top 10  
768 most significantly overlapping gene sets are shown from top to bottom. B) Scatter plot of  
769 genes identified to be up or down regulated in response to estradiol treatment, that are  
770 also bound by estrogen receptor α (ERα) and RUNX1 (empty circles, blue for  
771 downregulated and red for upregulated). Scatter plot also illustrates up or down  
772 regulated genes in response to estradiol treatment that are bound by ERα and  
773 mitotically bookmarked by RUNX1 (filled in circles, blue for downregulated and red for  
774 upregulated). C) Top panel: ChIP-Seq tracks of *HES1* (left) and *H2AFX* (right) from  
775 asynchronous (top-red), mitotic (middle-green), and G1 (bottom-blue). Bottom panel:  
776 qRT-PCR data of *HES1* (left) and *H2AFX* (right) in asynchronous MCF10A cells treated  
777 with either active (AI-14-91) or inactive (AI-4-88) inhibitors for 6hr, 12hr, 24hr and 48hr  
778 at 20μM. Expression of target genes were normalized relative to beta actin.

779

780 **Figure 6. Disrupting RUNX1 mitotic gene bookmarking in MCF10A cells leads to a**  
781 **transformed cellular phenotype and EMT.** A) Phase contrast microscopy images of  
782 MCF10A cells treated with AI-4-88 or AI-14-91 for 48hr at 20μM. Left panel – 4X  
783 magnification, middle panel – 20X magnification, right panel – 40X magnification.  
784 Outlined square in middle panel is the resulting 40X magnification in the right panel. B)  
785 Top Panel: Experimental schematic depicting treatment schedule for the “crisis” and

786 “recovery” stages. Bottom Panel: Phase contrast microscopy images from Day 0, 1, and  
787 2 of crisis where MCF10A cells were treated with AI-14-91 at 20 $\mu$ M (top – left, middle,  
788 right respectively). Phase contrast images from Day 0, 4, and 7 of recovery following a  
789 media replacement. C) Morphological changes upon inhibition of RUNX1-CBF $\beta$   
790 interaction are confirmed by examining localization of the cytoskeletal protein F-actin.  
791 When compared to inactive compound (top panel), cells treated with active compound  
792 show substantial alterations in cytoarchitecture (bottom panel). D) Western blot for  
793 epithelial marker E-Cadherin (top row), mesenchymal marker Vimentin (middle row),  
794 and loading control beta actin (bottom row) in MCF10A whole cell lysates harvested  
795 from cells treated with either inactive AI-4-88 (88) or active AI-14-91 (91) inhibitors at  
796 20 $\mu$ M for either 6, 12, 24, or 48hrs. E) qRT-PCR of target genes *p21* (RUNX1 regulated)  
797 and *SNAI2* (EMT inducing transcription factor) within asynchronous MCF10A cells  
798 treated with either inactive AI-4-88 (88) or active AI-14-91 (91) inhibitors at 20 $\mu$ M for  
799 either 6, 12, 24, or 48hrs. Expression of target genes were normalized relative to beta  
800 actin.

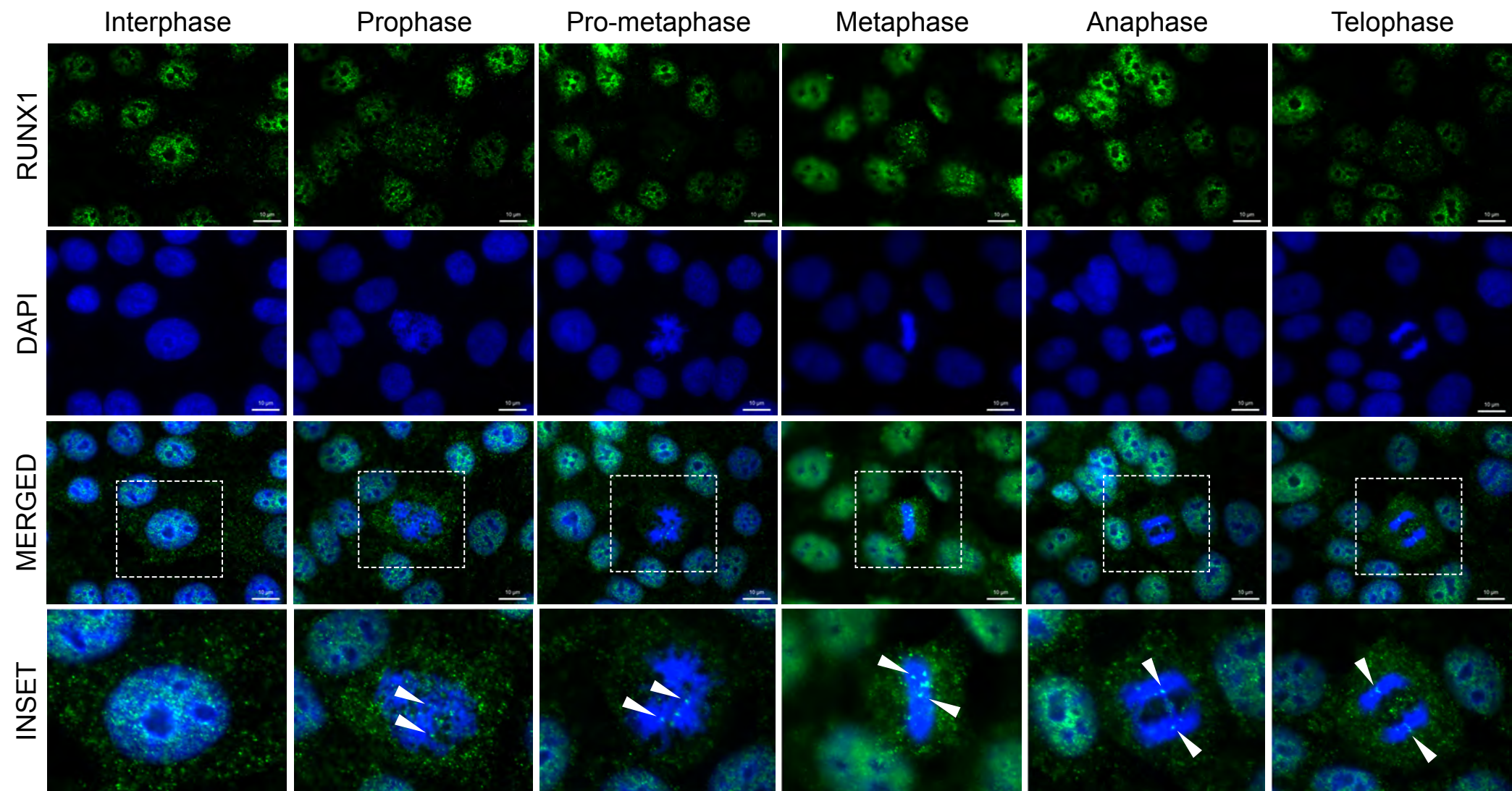
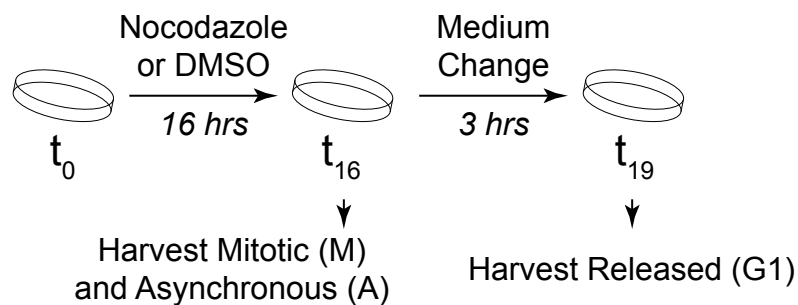
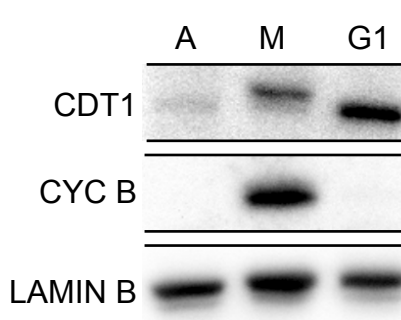


Figure 1

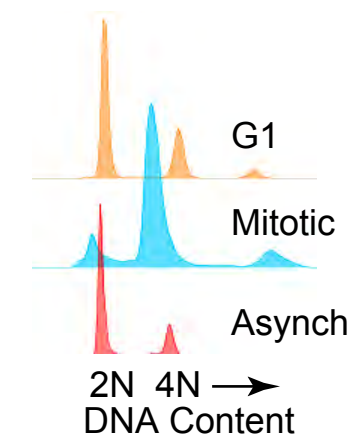
A.



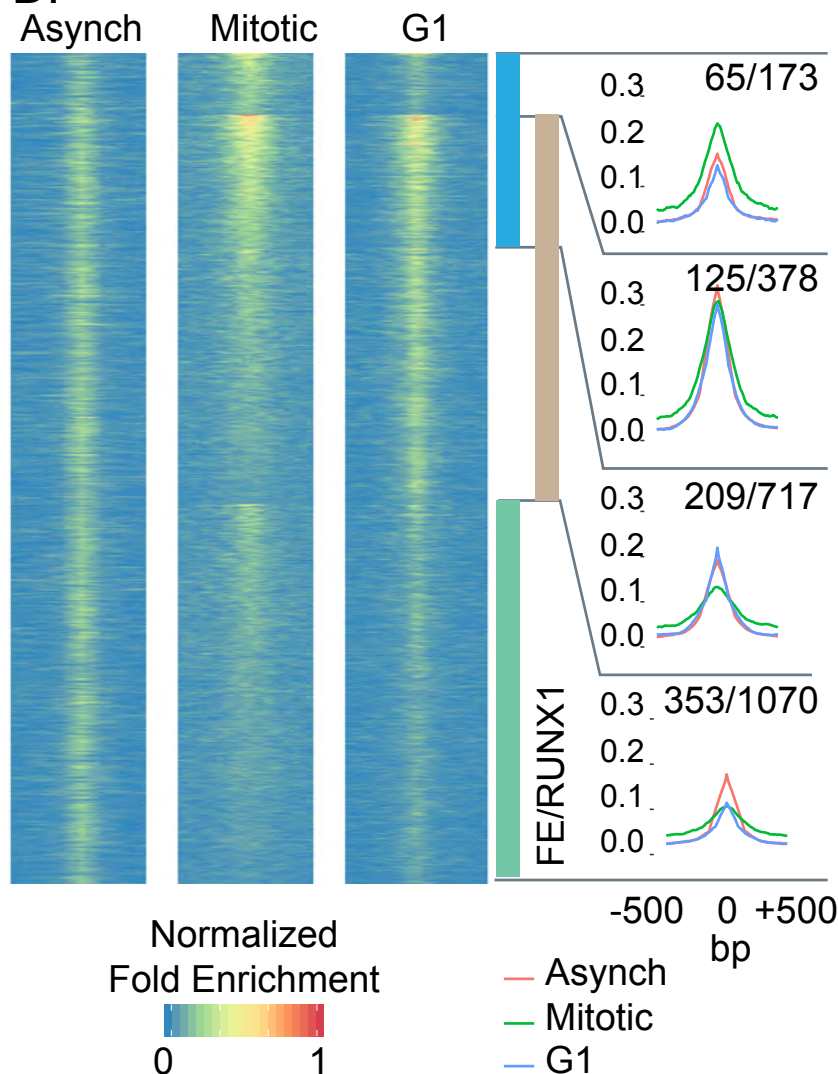
B.



C.



D.



E.

### Gene Ontology Analysis

Mitotic Bound	Negative Regulation of Gene Expression
G1 Bound	Negative Regulation of Metabolic Process
Not Bound in M or G1	Regulation of Response to Stress
	Regulation of Protein Localization
Mitotic	Anchoring Junction
	Positive Regulation of Gene Expression
	Protein Localization
	Cell Junction
G1	Enzyme Binding
	Protein Complex Subunit Organization
	Positive Regulation of Molecular Function
	Positive Regulation of Catalytic Activity

F.

Cell Type	Transcription Factor	Sequence Motif	P-value	% of Targets
Asynchronous	RUNX	GTAAACCGCAAG	1e-2350	54.71%
	JunB	GATGACTCAT	1e-446	15.90%
	ETS	CCACAGGAAT	1e-106	3.18%
Mitotic	RUNX	TTTGGCGGTTA	1e-521	52.96%
	JunB	GATGACTCAT	1e-50	10.94%
	TEAD2	ACAGGAATGC	1e-23	2.01%
G1	RUNX	CTGCTGGTTGCA	1e-1566	59.01%
	Fra1	ATGACTCACT	1e-260	19.61%
	ETS1	AGGATGTGGT	1e-51	4.32%

↑ P-value ↑ % of Targets

Figure 2

A. Interphase

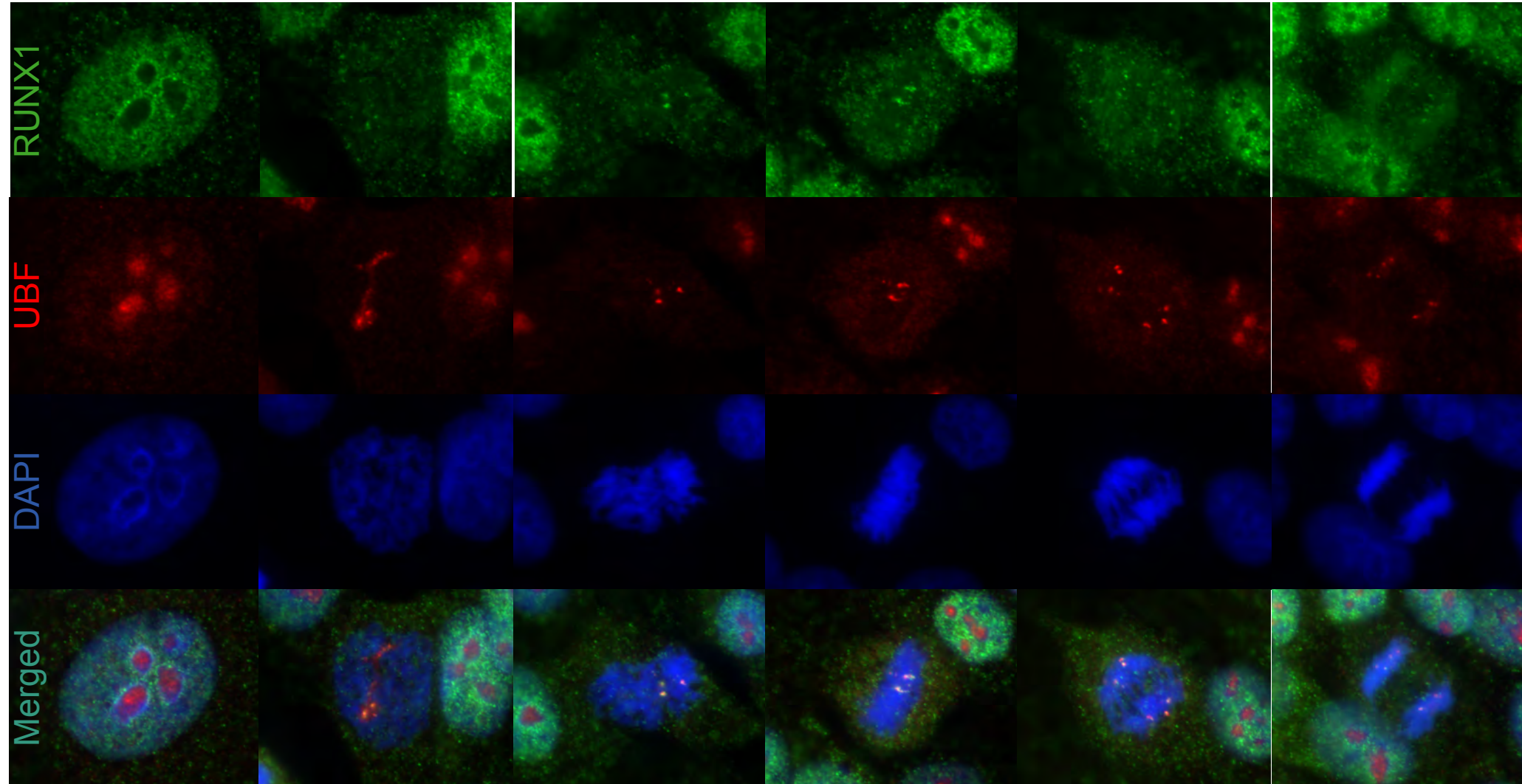
Prophase

Prometaphase

Metaphase

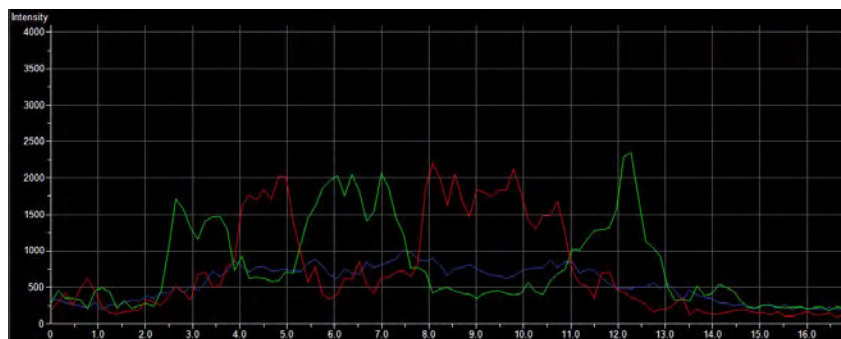
Anaphase

Telophase

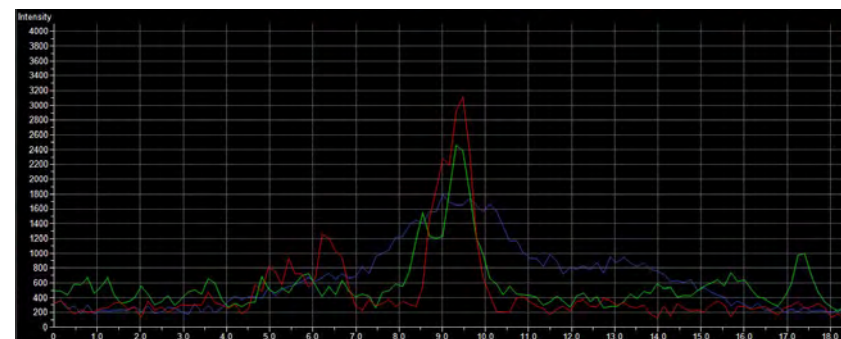


B.

Signal Overlay



Interphase



Metaphase

Figure 3

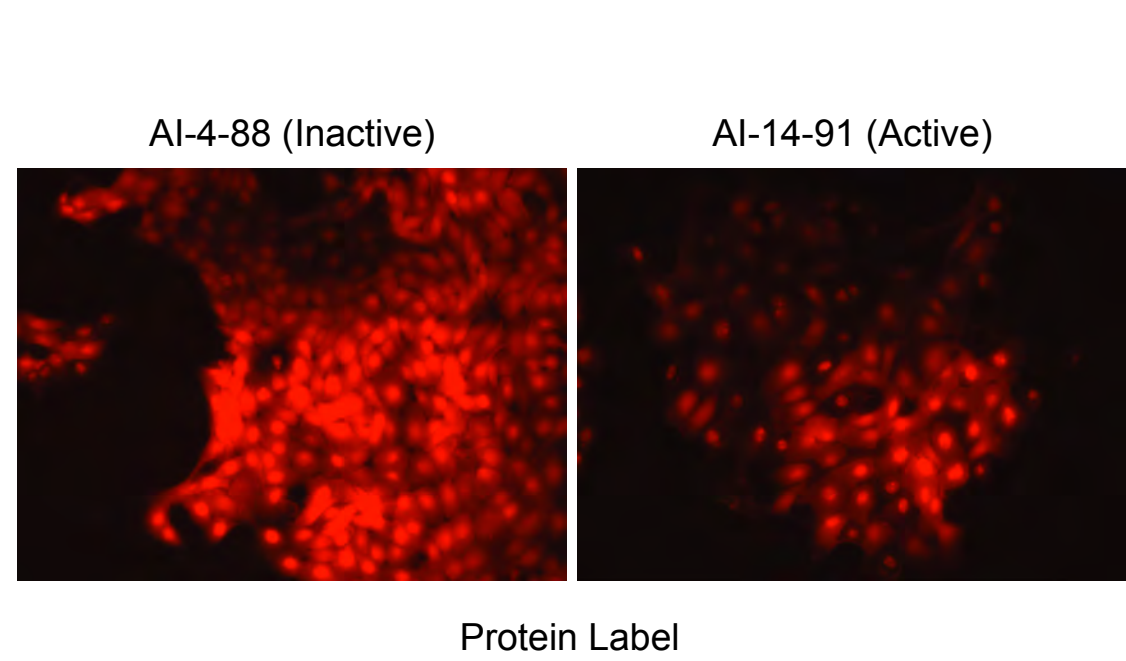
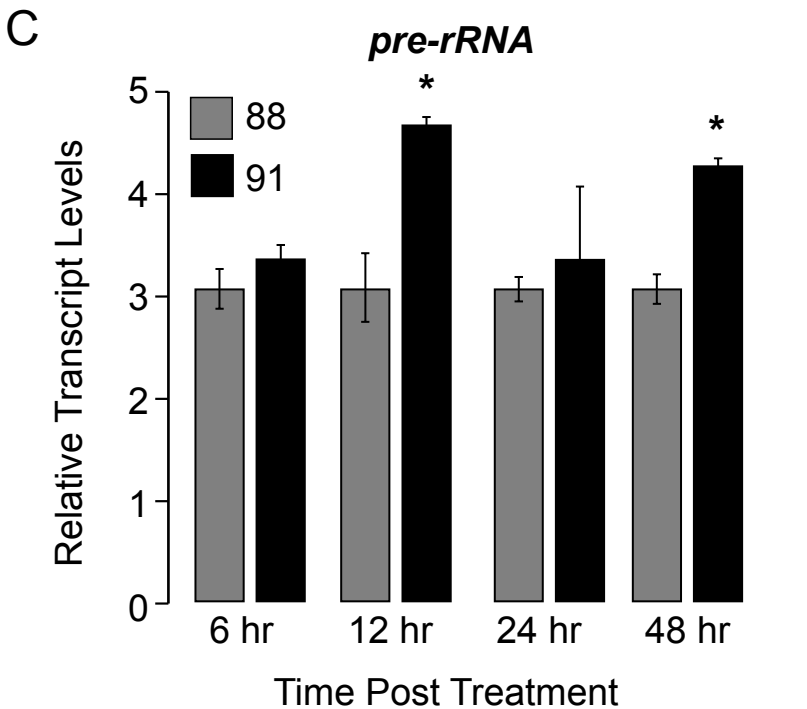
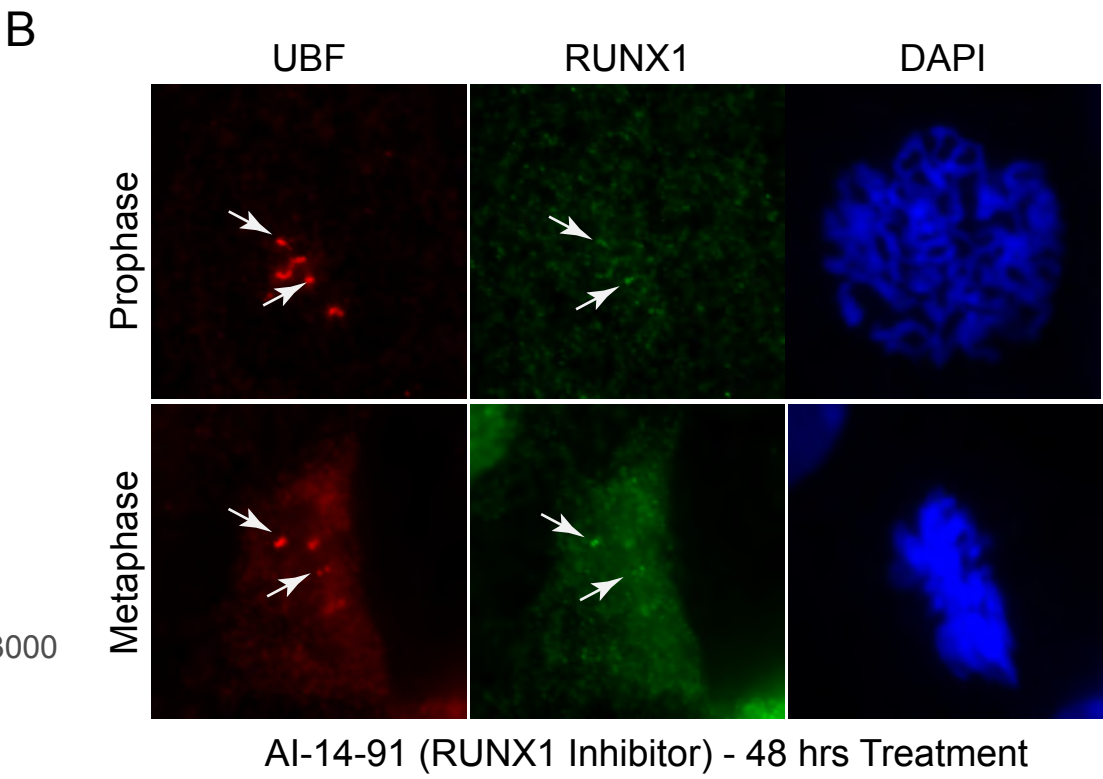
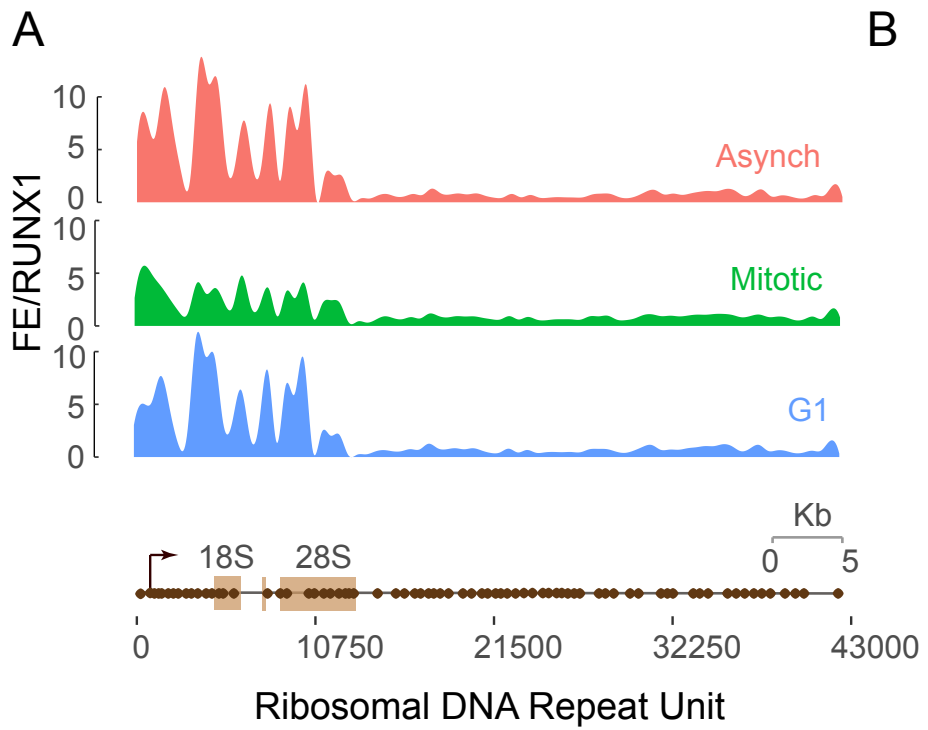


Figure 4

A

Gene Set Name [# of Genes]	# of Bookmarked Genes
HALLMARK_ESTROGEN_RESPONSE_LATE [200]	12
HALLMARK_MTORC1_SIGNALING [200]	12
HALLMARK_TNFA_SIGNALING_VIA_NFKB [200]	12
HALLMARK_APICAL_JUNCTION [200]	11
HALLMARK_ESTROGEN_RESPONSE_EARLY [200]	10
HALLMARK_G2M_CHECKPOINT [200]	10
HALLMARK_P53_PATHWAY [200]	10
HALLMARK_DNA_REPAIR [150]	8
HALLMARK_E2F_TARGETS [200]	9
HALLMARK_NOTCH_SIGNALING [32]	4

B

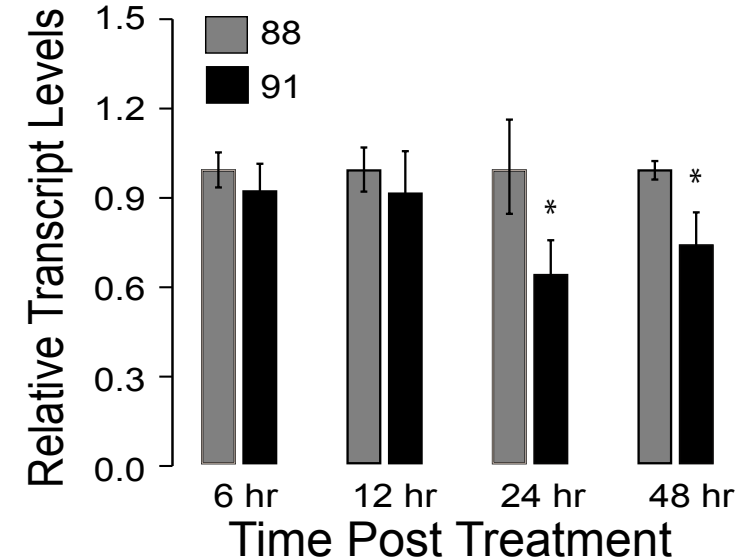
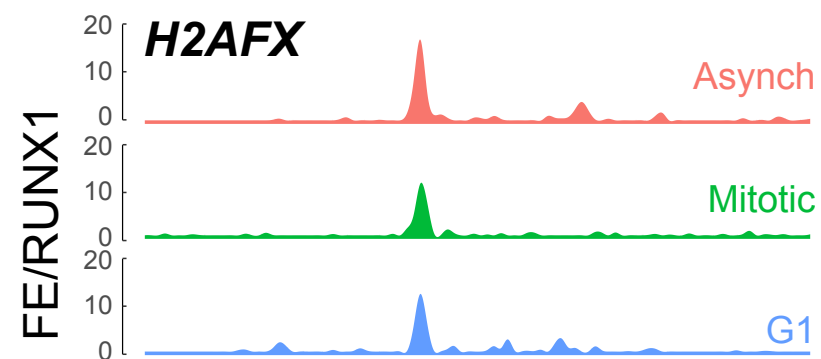
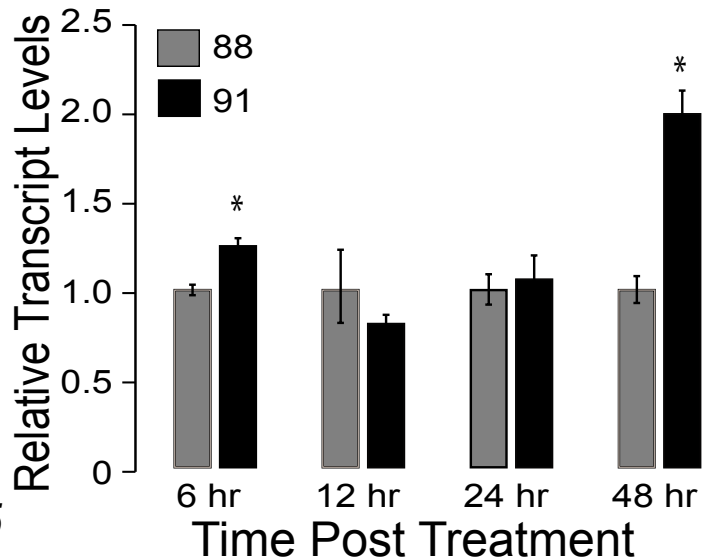
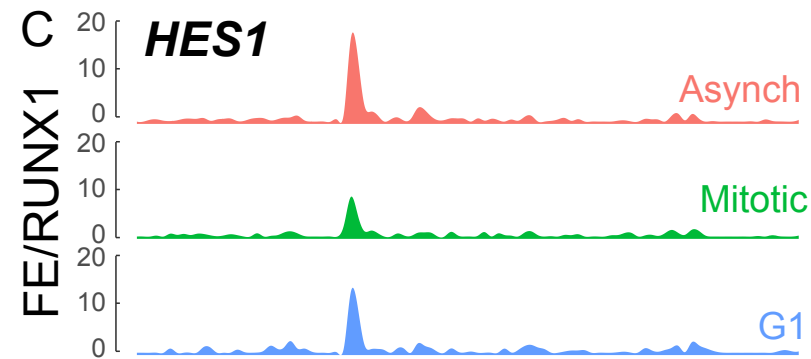
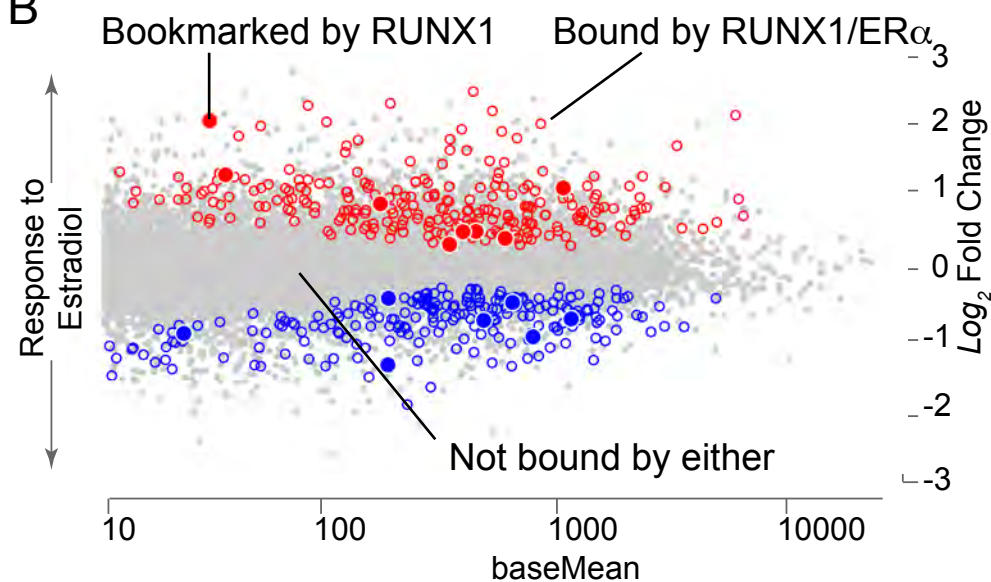
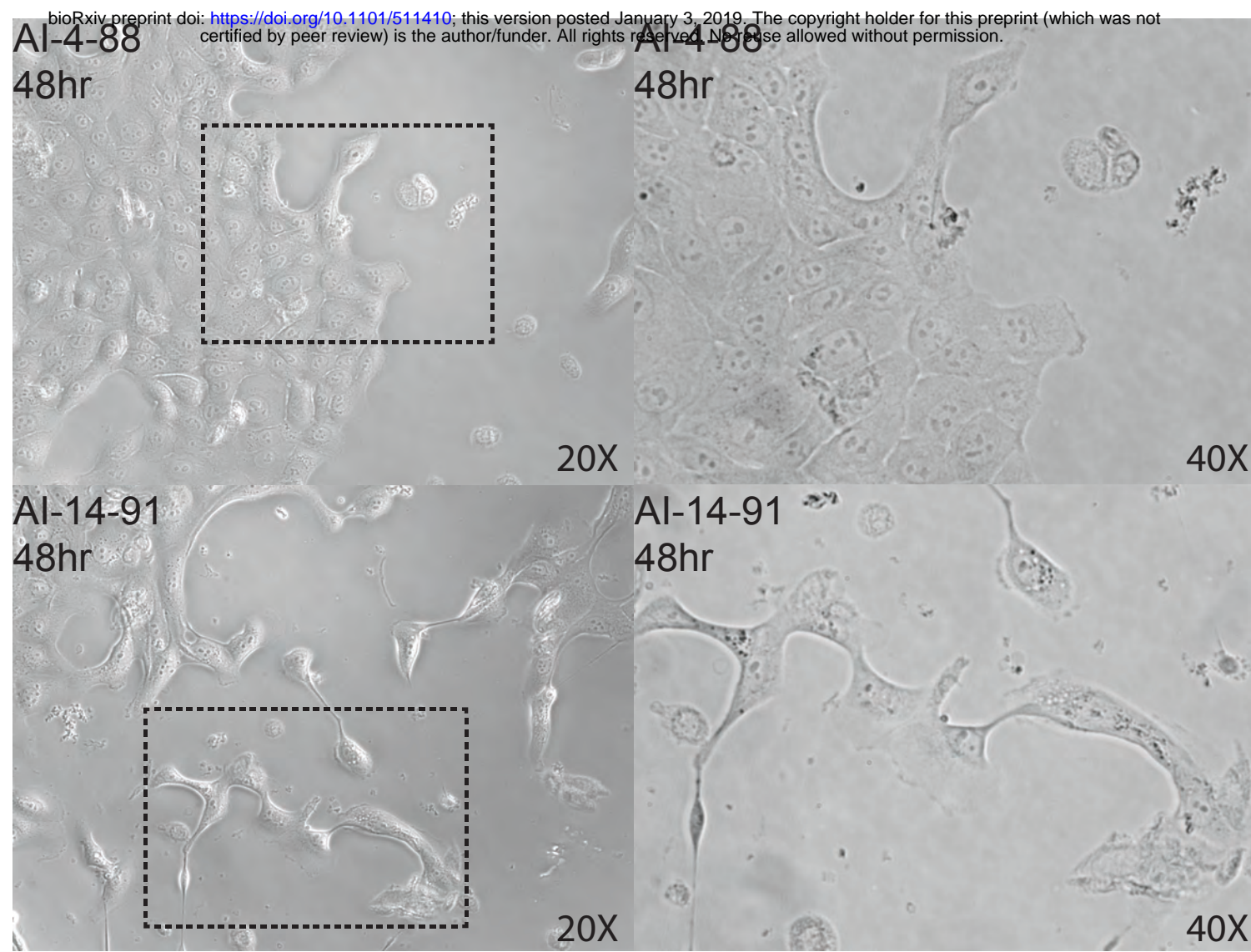
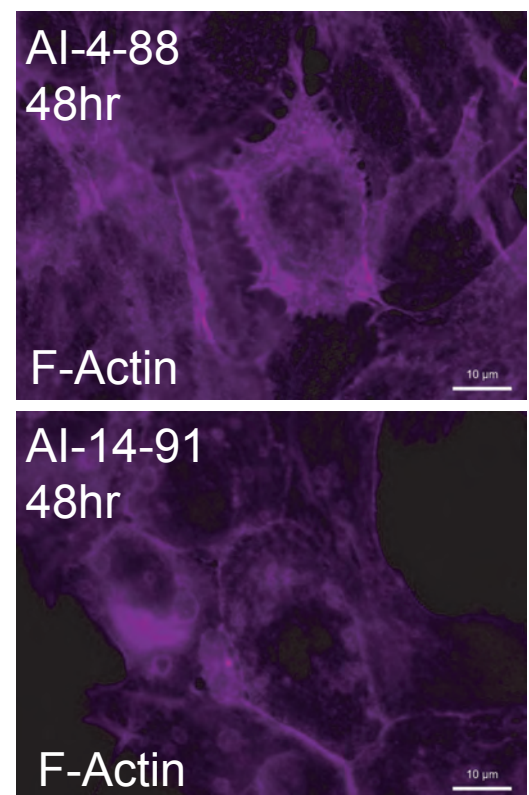
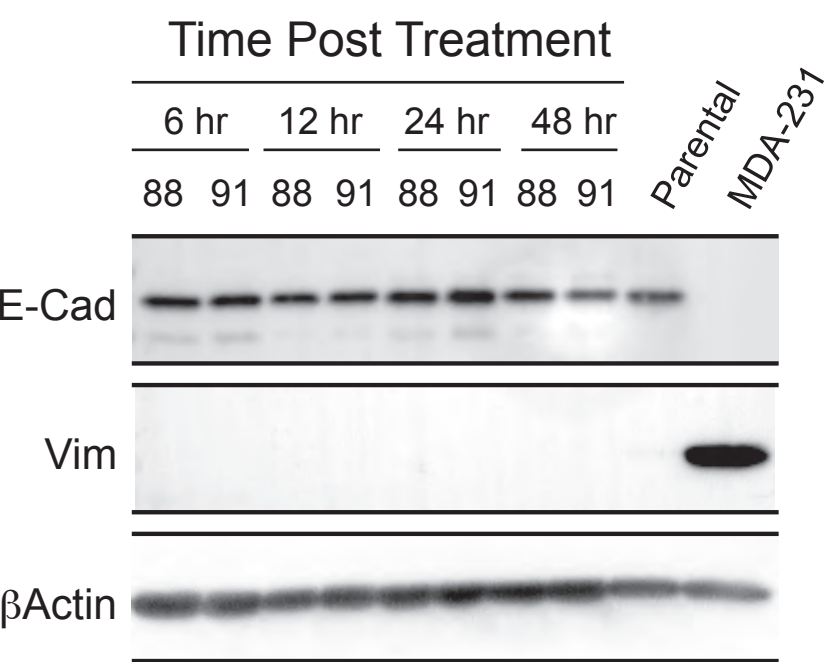
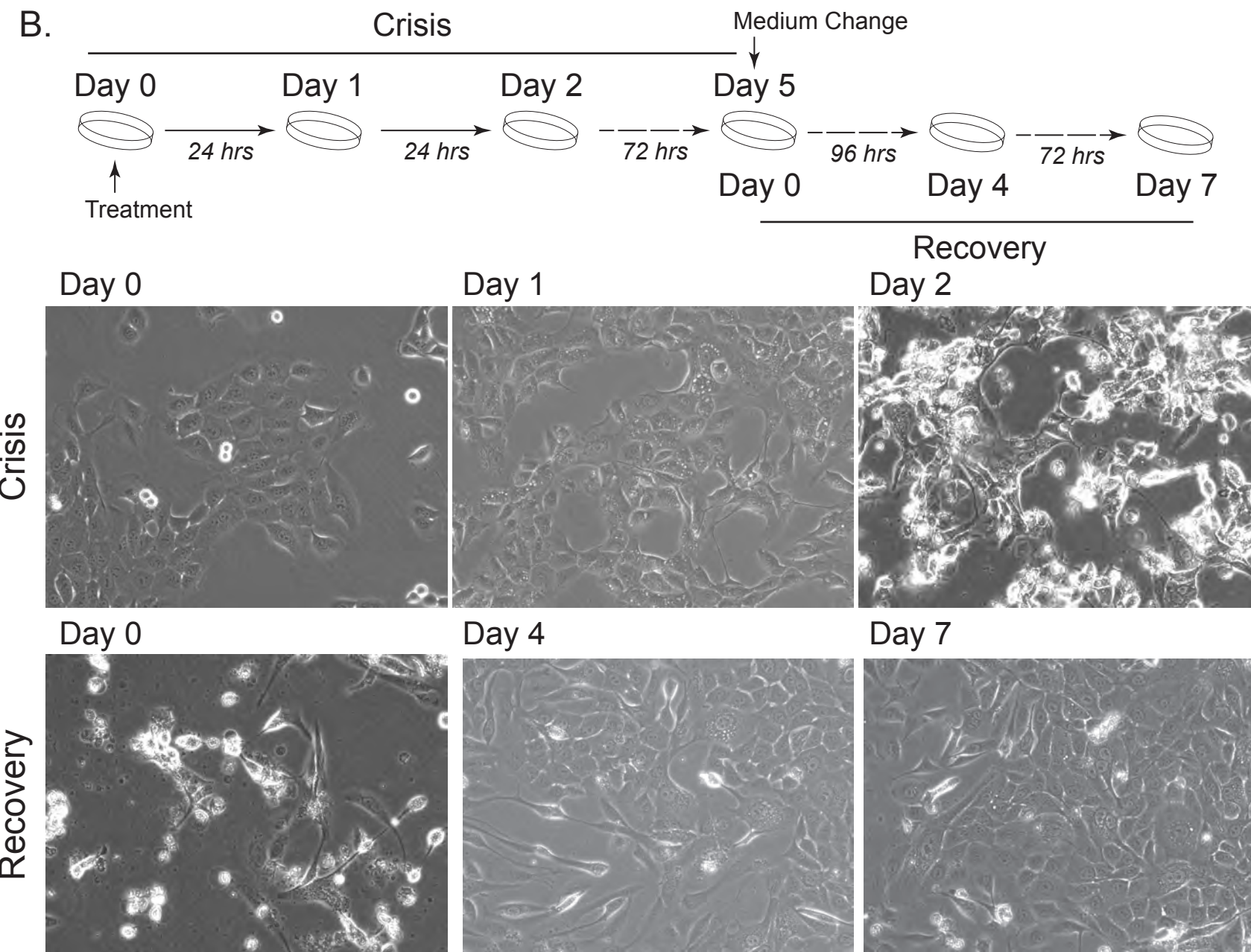
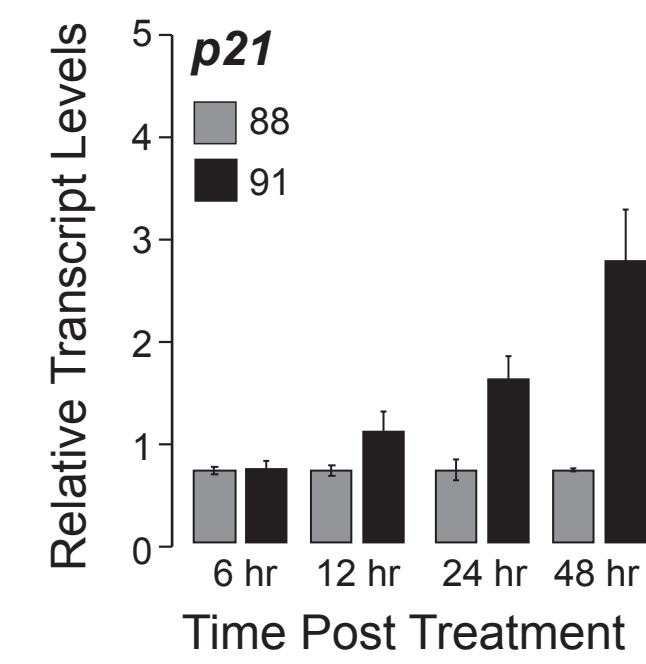
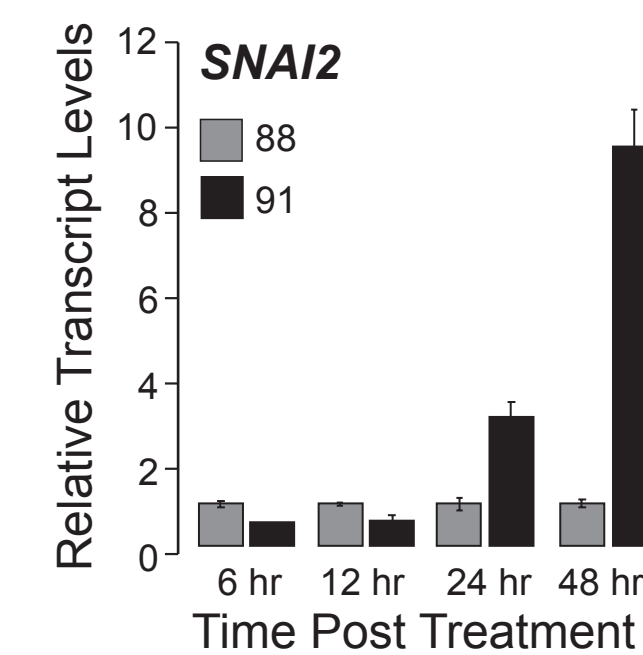


Figure 5

**A.****C.****D.****B.****E.****Figure 6**